

AD-774 389

AIR CUSHION LANDING SYSTEM PERFORMANCE ON A TENTH-SCALE MODEL JINDIVIK RPV

Philip M. Parker, Jr.

Air Force Institute of Technology
Wright-Patterson Air Force Base, Ohio

November 1973

DISTRIBUTED BY:

NTIS

National Technical Information Service
U. S. DEPARTMENT OF COMMERCE
5285 Port Royal Road, Springfield Va. 22151

Unclassified

Security Classification

14 KEY WORDS	LINK A		LINK B		LINK C	
	ROLE	WT	ROLE	WT	ROLE	WT
Air Cushion Landing System Tenth-scale model Jindivik drone Static stiffness tests Drop tests Catapult tests						

ia

Unclassified

Security Classification

AIR CUSHION LANDING SYSTEM PERFORMANCE

ON A TENTH-SCALE MODEL JINDIVIK RPV

THESIS

GAM/AE/73A-15

Philip M. Parker, Jr.
Captain USAF

Approved for public release; distribution unlimited.

APR 1974
RECEIVED

ib

AIR CUSHION LANDING SYSTEM PERFORMANCE
ON A TENTH-SCALE MODEL JINDIVIK RPV

THESIS

Presented to the Faculty of the School of Engineering
of the Air Force Institute of Technology

Air University

in Partial Fulfillment of the
Requirements for the Degree of
Master of Science

by

Philip M. Parker, Jr., B.S.

Captain USAF

Graduate Aerospace-Mechanical Engineering

November 1973

Approved for public release; distribution unlimited.

Preface

The testing and evaluation of air cushion landing system designs is a required step in the development and deployment of an operational system. The problems encountered in performing the tests on large scale vehicles, and the limitation on the number of designs which can be tested impose a severe handicap on the widespread development of this very promising system. This report represents my efforts to assess the feasibility of utilizing tests on small scale models to provide information useful to the development of larger scale systems.

The two major efforts of this study were to perform representative tests on the air cushion landing system of a tenth-scale model Jindivik RPV, and to compare the results of these tests with similar tests performed on a full-scale Jindivik air cushion landing system. The results of these efforts are published herein. Judged on the basis of my personal education and satisfaction, the success of this study was enormous; it is my hope that the results will prove beneficial to those involved with the design and construction of future air cushion landing systems.

I am deeply indebted to the personnel of the AFIT shop whose efforts in constructing and installing the test hardware made this report possible. The expert technical advice and assistance of Mr. Shade Campbell and Mr. David Pool were essential in the performance of the experiments of this study. Mr. Jim Steiger provided the

DOCUMENT CONTROL DATA - R & D

(Security classification of title, body of abstract and indexing annotation must be entered when the overall report is classified)

1. ORIGINATING ACTIVITY (Corporate author) Air Force Institute of Technology (AFIT-EN) Wright-Patterson Air Force Base, Ohio 45433	2a. REPORT SECURITY CLASSIFICATION Unclassified 2b. GROUP
--	---

3. REPORT TITLE
Air Cushion Landing System Performance on a Tenth-Scale Model
Jindivik RPV

4. DESCRIPTIVE NOTES (Type of report and inclusive dates)
AFIT Thesis

5. AUTHOR(S) (First name, middle initial, last name) Philip M. Parker, Jr. Capt USAF	Reproduced by NATIONAL TECHNICAL INFORMATION SERVICE U S Department of Commerce Springfield VA 22151
--	--

6. REPORT DATE November 1973	7a. TOTAL NO OF PAGES 71	7b. NO. OF REFS 3
---------------------------------	-----------------------------	----------------------

8a. CONTRACT OR GRANT NO. b. PROJECT NO. c. N/A d.	9a. ORIGINATOR'S REPORT NUMBER(S) GAM/AE/73A-15 9b. OTHER REPORT NO(S) (Any other numbers that may be assigned this report)
---	---

10. DISTRIBUTION STATEMENT
Approved for public release; distribution unlimited.

11. SUPPLEMENTARY NOTES Approved for public release; IAW AFR 190-17 JERRY C. HIX, Captain, USAF Director of Information	12. SPONSORING MILITARY ACTIVITY Air Force Flight Dynamics Laboratory Wright-Patterson AFB, Ohio 45433 AFFDL/FEM
--	---

13. ABSTRACT

Tests were conducted on an air cushion landing system ACLS installed on a tenth-scale model Jindivik RPV. The model has the correct Froude-scaled values of weight, center of gravity cg and moment of inertia about all three axes. The results of these tests were compared to the results of similar tests conducted on the ACLS of a full-scale model Jindivik.

Static tests on the tenth-scale ACLS determined the heave stiffness to be 11 lb per in., the pitch stiffness to be .155 lb ft per deg (for a nose down moment) and the roll stiffness to be .0048 lb ft per deg. These values were within 60% of the full-scale values.

Drop tests showed the maximum load at the cg of the model to vary between 2.2 g's at the scaled nominal landing rate of descent, to 5.4 g's at the maximum landing rate of descent. Comparison between systems at the nominal landing rate of descent show the load dynamics to be similar. The pressure dynamics of the tenth-scale system showed no correlation with the full-scale ACLS data.

At launch speeds of 8 mph and 12 mph, high speed films of the catapult tests showed that the tenth-scale Jindivik had less pitch oscillations after touchdown with the air cushion vented than in the normal landing configuration. Touchdowns at higher speeds were not analyzed due to the narrow field of view of the high speed camera.

necessary liason between my program of tests and that of the full-scale Jindivik.

My special thanks go to Maj. John C. Vaughan, Chief Scientist of the Mechanical Branch, Vehicle Equipment Division, Air Force Flight Dynamics Laboratory, whose encouragement and guidance are chiefly responsible for whatever success was achieved in this program.

I would also like to express my appreciation to Dr. Andrew J. Shine, Prof. Harry R. Bulmer and Capt J. T. Karam, Jr., my advisors, for their advice and suggestions and for the many hours, freely given, to assist me in preparing this report.

Philip M. Parker, Jr.

Contents

	<u>Page</u>
Preface	ii
List of Figures	vi
List of Tables.	vii
List of Symbols	viii
Abstract.	x
I. Introduction	1
Purpose	1
Background.	1
Definition of Terms	4
Scope	5
II. Apparatus.	7
Tenth-Scale Model Jindivik.	7
Catapult.	9
Test Instrumentation.	9
III. Test Configuration for Tenth-Scale ACLS.	11
Scale Considerations.	11
Air Supply System	12
Center of Gravity Considerations.	12
Pull Tests.	15
IV. Static Tests	16
Heave Stiffness	16
Pitch Stiffness	18
Roll Stiffness.	19

	<u>Page</u>
V. Drop Tests	22
Instrumentation	22
Results of Drop Tests	22
VI. Catapult Tests	25
Launch Velocity	25
Separation from the Catapult Carriage	25
Configuration	26
Braking Coefficient	27
VII. Conclusions and Recommendations.	28
Conclusions	28
Recommendations	29
Bibliography	31
Appendix A: Scale Verification	32
Appendix B: Small Scale ACLS Trunk Manufacture	33
Appendix C: Catapult Design.	35
Appendix D: Instrumentation.	36
Appendix E: Summary of Test Data	39
Appendix F: Calculations and Error Analysis.	55
VITA	61

List of Figures

<u>Figure</u>		<u>Page</u>
1	Schematic of ACLS Trunk	3
2	Cross Section of ACLS Viewed from the Front	4
3	Tenth-Scale Model Jindivik.	8
4	Diagram of Catapult System.	10
5	ACLS Pressure Response to Trunk Flow Area Change.	13
6	Performance of Air Supply System.	14
7	ACLS Deflection With Load Over the cg for Landing Configuration	17
8	Effect of Pitching Moment on ACLS Pitch Attitude.	20
9	Effect of Rolling Moment on ACLS Bank Angle	21
10	Sample Drop Test Schematic.	24
11	Adverse Pitch Moments at Touchdown.	27
12	ACLS Trunk.	34
13	Deflection of ACLS With Load for Cushion Vented Landing Configuration	45
14	Deflection of ACLS With Load for Take Off Configuration	47
15	Deflection of ACLS With Load for Cushion Vented Take Off Configuration	49

List of Tables

<u>Table</u>	<u>Page</u>
I Scaled Values for Tenth-Scale Jindivik Design	32
II Trunk Pressure and Flow Rate vs Trunk Flow Area	41
III ACLS Pressure Response as a Function of Trunk Flow Area .	42
IV Deflection of cg with Increased Load for Landing Configuration	43
V Deflection of cg with Increased Load for Landing Configuration with Air Cushion Vented	44
VI Deflection of cg with Increased Load for Take Off Configuration	46
VII Deflection of cg with Increased Load for Take Off Configuration, Air Cushion Vented	48
VIII Results of Pull Tests	48
IXa Roll Angle of ACLS for Positive Torque Applied About the Longitudinal Axis	50
IXb Roll Angle of ACLS for Negative Torque Applied About the Longitudinal Axis	50
Xa Pitch Angle of ACLS for Positive Torque Applied About the lateral Axis.	51
Xb Pitch Angle of ACLS for Negative Torque Applied About the Lateral Axis.	51
XI Results of Drop Tests Using Bell and Howell Accelerometer	52
XII Results of Drop Tests Using BBN-501 Accelerometer	53
XIII Braking Factor for Landings with Air Cushion Vented . . .	54
XIV Theoretical Values of Air Cushion Area.	54

List of Symbols

<u>Symbol</u>	<u>Description</u>	<u>Unit</u>
a_c	Acceleration of Catapult Carriage	ft/sec ²
a_d	Deceleration of Model During Landing Slide	ft/sec ²
a_{cg}	Acceleration of the Vehicle Center of Gravity	ft/sec ²
ACLS	Air Cushion Landing System	--
A_c	Cushion Area	in. ²
A_t	Trunk Area	in. ²
A_{11}	Trunk Flow Area	in. ²
b	Span	in.
C_d	Discharge Coefficient	--
cp	Center of Pressure	--
d_s	Distance of Landing Slide	ft
F_p	Pull Force	lbf
g_c	Dimensional Constant	ft-lbm/lbf-sec ²
H	Height	in.
IGE	In Ground Effect	--
K_h	Heave Stiffness Factor	lb/in.
K_θ	Pitch Stiffness Factor	lb-ft/deg
K_ϕ	Roll Stiffness Factor	lb-ft/deg
L	Length	in. or ft
OGE	Out of Ground Effect	--
P_a	Atmospheric Pressure	psia
P_c	Cushion Pressure	psig or in. H ₂ O(gage)

<u>Symbol</u>	<u>Description</u>	<u>Unit</u>
P_t	Trunk Pressure	psig or in. H_2O (gage)
Q	Flow Rate	cfm
R	Radius	in.
t	Time	sec
t_c	Time for Full Carriage Travel	sec
u	Velocity	fps
V_L	Launch Velocity	fps
V_V	Vertical Descent Rate	fps
W	Weight	lbf
ΔH	Measured Change in Height	in.
P_a	Standard Atmospheric Density	lbm/ft
μ	Braking Factor	---

AIR CUSHION LANDING SYSTEM PERFORMANCE
ON A TENTH-SCALE MODEL JINDIVIK RPV

I. Introduction

Purpose

The purpose of this study was to experimentally determine the performance of an air cushion landing system installed on a tenth-scale model Jindivik RPV. The performance of the system was evaluated from determination of the following:

1. Static stiffness of the air cushion landing system in level, pitch and roll attitudes.
2. Dynamic response of the system to the effect of vertical velocity during landing.
3. Landing stability of the system at various forward speeds at different air flow configurations.

A number of the measurements of the tenth-scale system's performance were compared with similar measurements of an air cushion landing system installed on a full-scale model Jindivik. This comparison has provided some answers to questions concerning the feasibility of using data, obtained from tests on a small model (the model of this study weighed 2.5 lb), in designing air cushion landing systems.

Background

The basic ACLS consists of a trunk which is shaped, as shown in Fig. 1, like an elongated doughnut or toroid, and an air supply system. The trunk is attached to the bottom of the aircraft fuselage and is

inflated by air from the air supply system. The compressed air may be allowed to escape from many small holes along the bottom and inner surface of the trunk. The air escaping from these holes generates and maintains a pressure increase in the cushion region of 1 to 4 psi above atmospheric which forms an air cushion upon which the vehicle rides. (Ref 21) This air cushion supports the weight of the aircraft over a relatively large surface area. The light footprint thus created allows the vehicle to operate on unprepared surfaces such as sod, snow, sand or water. In addition to this flexibility an overall weight savings can be realized in comparison with conventional landing gear systems.

The many interacting variables of air cushion landing system operation make theoretical prediction of ACLS performance very difficult. At the time of this writing there are no proven analytical methods for predicting the performance of a particular ACLS, and scale model testing remains the primary method for providing information necessary for design verification. A small model could provide ACLS data at a considerable savings in time and money but the similarity in operation between the small scaled model and full-scale system is open to question. AFFDL is currently conducting static and drop tests on the ACLS of a full-scale model Jindivik RPV. These tests are being conducted in preparation for a joint USAF, effort to perform ground/flight tests on an ACLS equipped Jindivik drone. It is the intent of this report that the comparison between the tenth-scale and full-scale systems will aid in determining if small models (on the order of 5 lb) can be used to develop data useful to full-scale ACLS design.

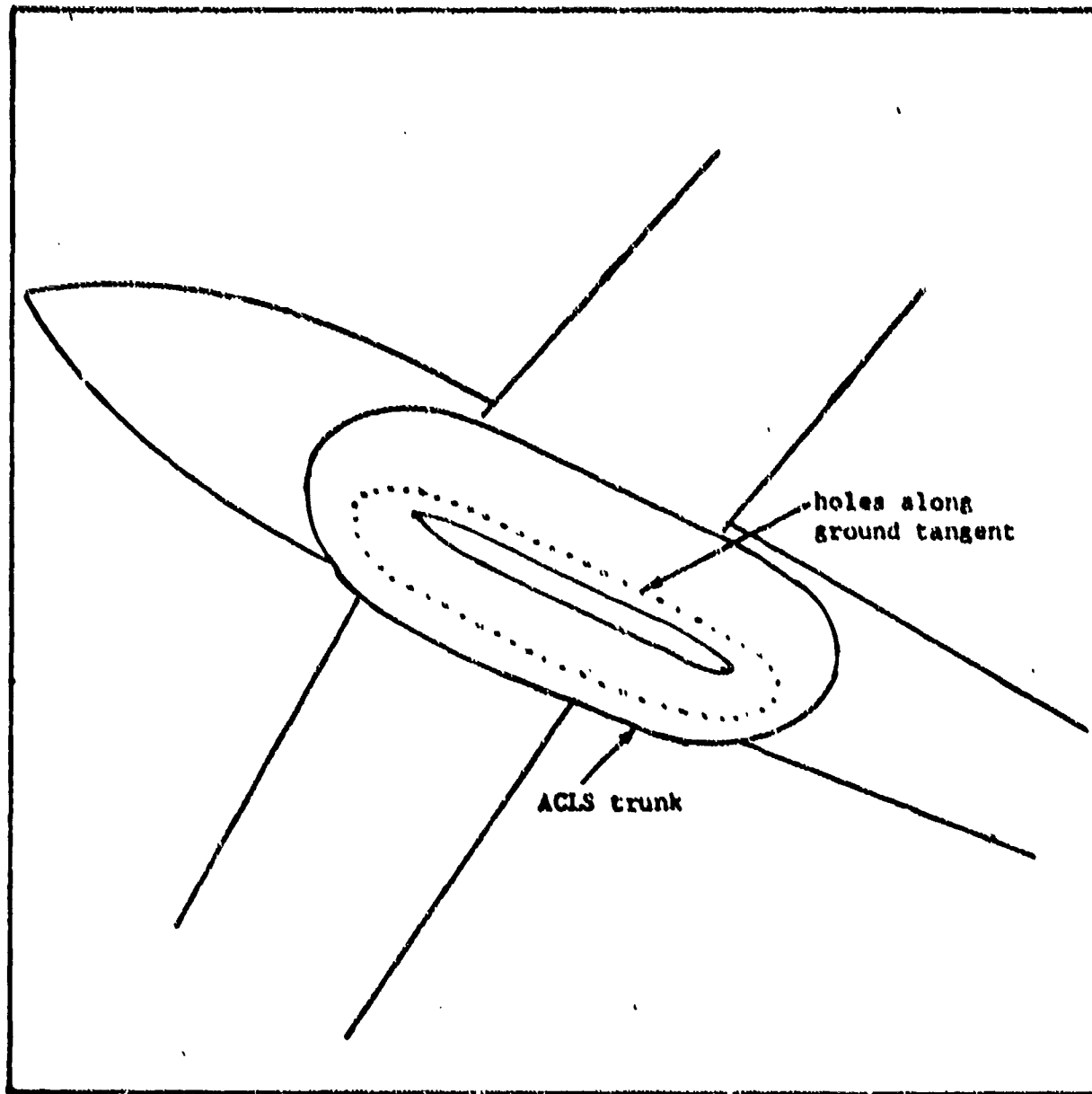


Fig. 1. Schematic of ACLS Trunk

Definition of Terms

Trunk Pressure P_t . That pressure, measured in terms of gage pressure, which exists within the toroid shaped trunk. This pressure tends to keep the trunk inflated during all ACLS operations.

Cushion Pressure P_c . The pressure, measured in terms of gage pressure, which exists exterior to the trunk, in the region bounded by the trunk and the fuselage as shown in Fig. 2.

Trunk Area A_t . That area of the trunk in contact with the ground or flattened by the effect of the ground at a given time and condition.

Cushion Area A_c . That area enclosed by the interior ground tangent line of the trunk surface in contact with the ground. In hover most of the vehicle weight is supported by P_c acting over the cushion area A_c .

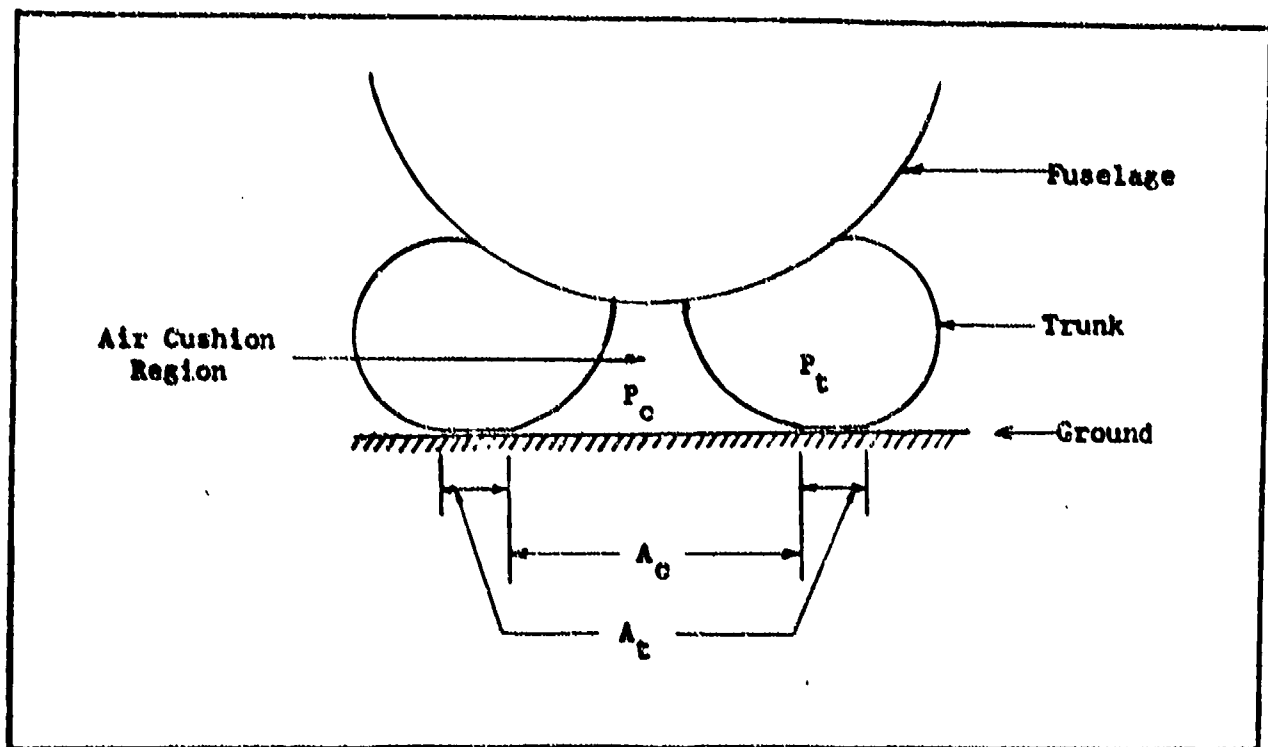


Fig. 2. Cross Section of ACLS Viewed from the Front

Center of Pressure cp . The geometric center of A_c .

Trunk Flow Area A_n . The total area of the ports in the trunk which allow air to flow out of the trunk and into the air cushion region. The effective trunk flow area is computed by multiplying the measured area A_n by a discharge coefficient C_d .

Ground Effect. The ground effect is determined by the effect of the ground on cushion pressure. When P_c is equal to the atmospheric pressure (zero gage pressure), the ACLS is said to be out of ground effect OGE. As P_c rises above atmospheric pressure the ACLS is in ground effect IGE with a nominal design point occurring when the vehicle is at rest on the ground with its weight being supported by the force of $P_c A_c$ and $P_c A_c$. This latter condition is referred to as hover. All tests on the tenth-scale Jindivik, except where noted otherwise, were conducted in ground effect.

Scope

Tests were conducted on a tenth-scale model Jindivik RPV equipped with an air cushion landing system. The experiments conducted did not yield the data necessary to describe the entire range of performance of the ACLS but a comparison of the data obtained, with similar results of AFFDL tests of the full-scale ACLS, provides a good indication of the validity of using a small model to provide data for ACLS development.

Static tests to determine the trunk stiffness in heave, pitch and roll were conducted. The determined values were compared against full-scale stiffness factors to determine the static similarity between systems.

The effects on the ACLS of the vertical velocity of landing were examined in a series of drop tests. The drop height was varied to give a range of vertical velocities to simulate full-scale values from the nominal landing rate of descent of 7.6 fps to the maximum expected rate of descent of 14 fps. The effects on the ACLS of varying the roll and pitch attitude in drop tests, were not studied.

Forward speed landing tests for a range of forward velocities from 12 to 30 fps, were accomplished through the use of a catapult. The motion of the model immediately after touchdown was studied through the use of high speed motion pictures. The braking performance of the ACLS was analyzed and compared with full scale data.

II. Apparatus

The primary piece of equipment used in this program was the tenth-scale model Jirdivik. The catapult used in the forward speed landing tests was built and installed by the AFIT shop. Its design is discussed in Appendix C. The primary instruments for most of the testing were two water manometers used to measure trunk pressure and cushion pressure. For the drop tests two pressure transducers and an accelerometer were used in recording the dynamic response of the ACLS. A high speed movie camera recorded the launch and touchdown in the catapult tests.

Tenth-Scale Model Jirdivik

The model was designed by Maj John C. Vaughan of AFFDL and Dr Ned Smith of Centro Aviation of Dayton, Ohio. Centro Aviation was responsible for the construction of the model. It has the correct Froude-scaled values of weight, center of gravity and moment of inertia about all three axes. The air supply system for the ACLS consists of two Rotron Aximax 2H fans which can supply up to 40 cfm of air at .15 psig to the trunk and cushion. A dump valve in the belly of the fuselage permits venting of the air cushion for tests of braking performance. A rotron Propimax 2 fan is installed in the aft section of the fuselage to provide aerodynamic force on a remotely controlled steering vane in the tail section. This steering vane provides heading control during taxi and forward speed tests. As shown in Fig. 3, the model dimensions are: wing-span 25 in., length 26½ in., weight 2.5 lb. The fuselage is constructed of molded fiberglass with magnesium bulkheads. The wings are made of balsa wood with aluminum attachments. The power system

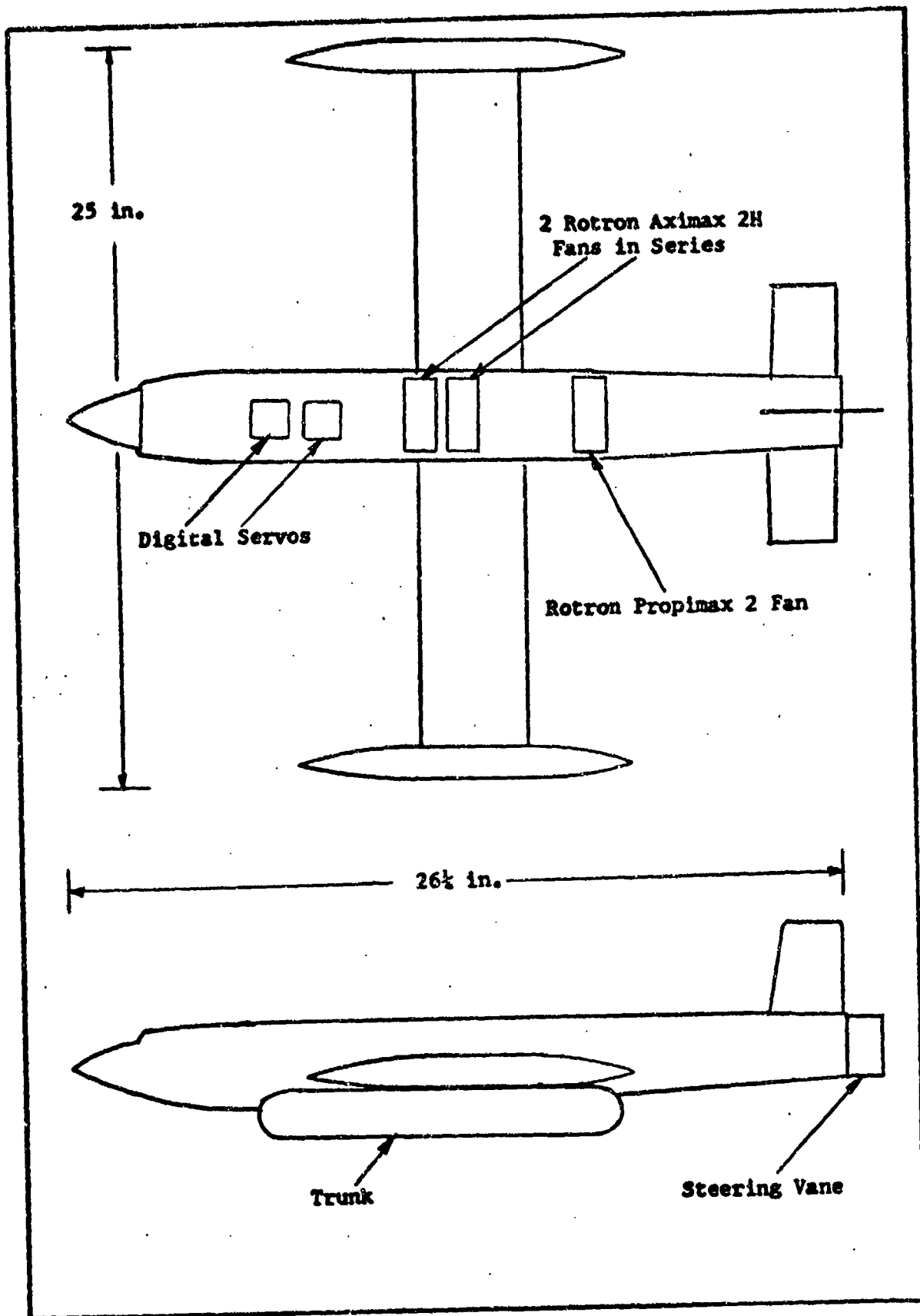


Fig. 3. Tenth-Scale Model Jindivik

was designed for a 110 volt 60 cycle electrical source. It provides 150 watts at 115 VAC 400 Hz through an umbilical cord. The power is adjustable through a voltage range of 105 to 125 VAC and a frequency range of 360 to 440 Hz. The control system consists of two digital proportional feedback servos which allow variable positioning of the cushion vent valve and steering vane. The trunk of the ACLS is a toroidal configuration and is scaled from a preliminary design of the trunk used in the full-scale ACLS. It is made of latex rubber and can have any desired hole pattern.

Catapult

The catapult shown in Fig.4 uses two 24 ft, 5 in. channel aluminum beams as launching rails. The rails are mounted on two height-adjustable stands which allow the model to be released at the proper attitude and altitude. The model is suspended from a carriage which rolls freely along the aluminum rails. The carriage is accelerated to the desired launching speed by a weight and pulley system; the model is then launched when the carriage strikes a padded block at the end of the rails.

Test Instrumentation

The test instrumentation for static tests included two water manometers and steel rule. Force measurements in the pull tests were made with a spring type load gage connected to the model by a system of pulleys. The instrumentation for the drop tests consisted of two strain gage type pressure transducers and a lightweight accelerometer. The signals from these instruments were conditioned and displayed on an oscillograph. Appendix D discusses the instrumentation in more detail.

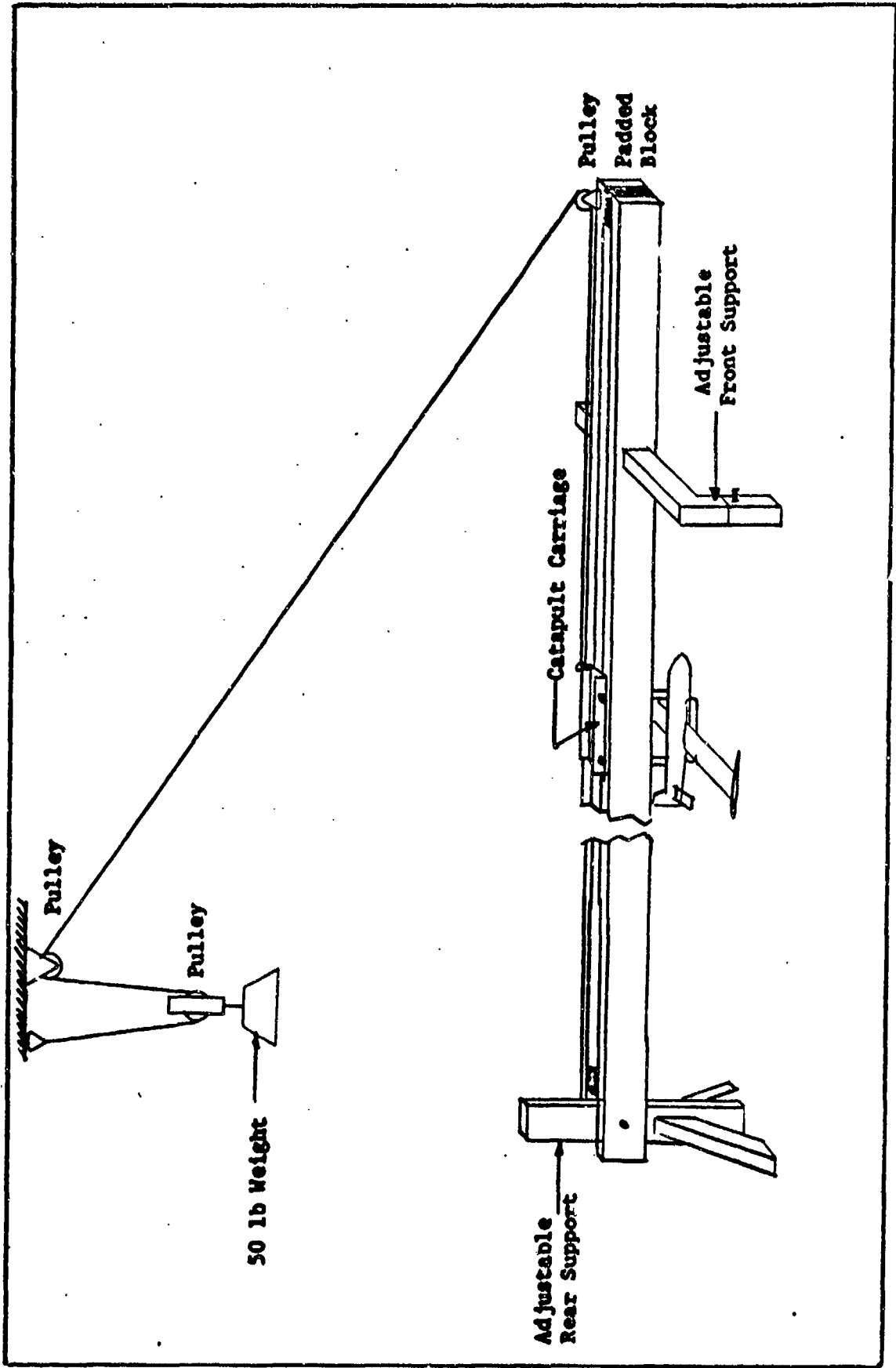


Fig. 4. Diagram of Catapult System

III. Test Configuration for Tenth-Scale ACLS

The goal in trimming the tenth-scale ACLS was to match as closely as possible scaled values from the full-scale system. The Jindivik ACLS was the first to be designed with different configurations for take off and landing. The system being tested on the full-scale model is a low air flow system which duplicates the designed landing configuration. This was to be the primary test configuration, however tests were conducted at a number of configurations to determine the overall performance of the system.

Scale Considerations

The size and shape of the tenth-scale trunk were properly proportioned, however the weight and thickness of the latex rubber were far greater than the correct scaled values. The difficulty in building a properly scaled trunk is one of the problems in using a small model to test an ACLS.

The operational parameters which had to be considered in trimming the ACLS were trunk pressure, cushion pressure, flow rate and trunk flow area. Trunk pressure was selected as the basic parameter in determining the desired test configuration. For a full-scale value of P_t of 1.7 psig (the pressure used in a series of full-scale tests) it was determined that the tenth-scale trunk pressure should be 4.75 in. H_2O . (See Appendix A for scale factors) The full scale tests employed a number of different configurations and ratios of P_c/P_t but a typical ratio was .38. For $P_t = 4.75$ in. H_2O the value of P_c for this ratio is 1.8 in. H_2O . Trunk and cushion pressures for the model

were measured for a number of flow areas at fan powers of 105 VAC 360 Hz, 115 VAC 400 Hz and 125 VAC 440 Hz as shown in Fig. 5. The operating condition at which the trunk and cushion pressures were closest to their properly scaled values was selected as the desired landing configuration. It was found that cushion pressure increased to a maximum value at a fairly low flow area and then remained essentially constant while trunk pressure decreased as flow area was increased. The pitch stability of the system was examined by observing the pitch damping of the system after being disturbed from equilibrium. It was found that a fairly large region of undamped or unstable operation exists, but the selected landing configuration was well removed from the area of unstable operation.

Air Supply System

The operating characteristics for a single Rotron Aximax 2H fan indicate an inherently unstable operating region, shown in Fig. 6. The pressure vs flow rate relation of 2 fans in series, as used in the model of this study, were found by measuring P_c out of ground effect at a number of different trunk flow areas and then computing the flow rate. (See Appendix F for sample computations.) The operating characteristics of this air supply system, shown in Fig. 6, do not indicate any region of unstable operation.

Center of Gravity Considerations

On the full-scale Jindivik the center of pressure of the ACLS is located 8.5 in. forward of the center of gravity. This was done partly to help counteract a nose down pitching moment encountered in landing. Since this nose down moment, due to the friction of the ground on the

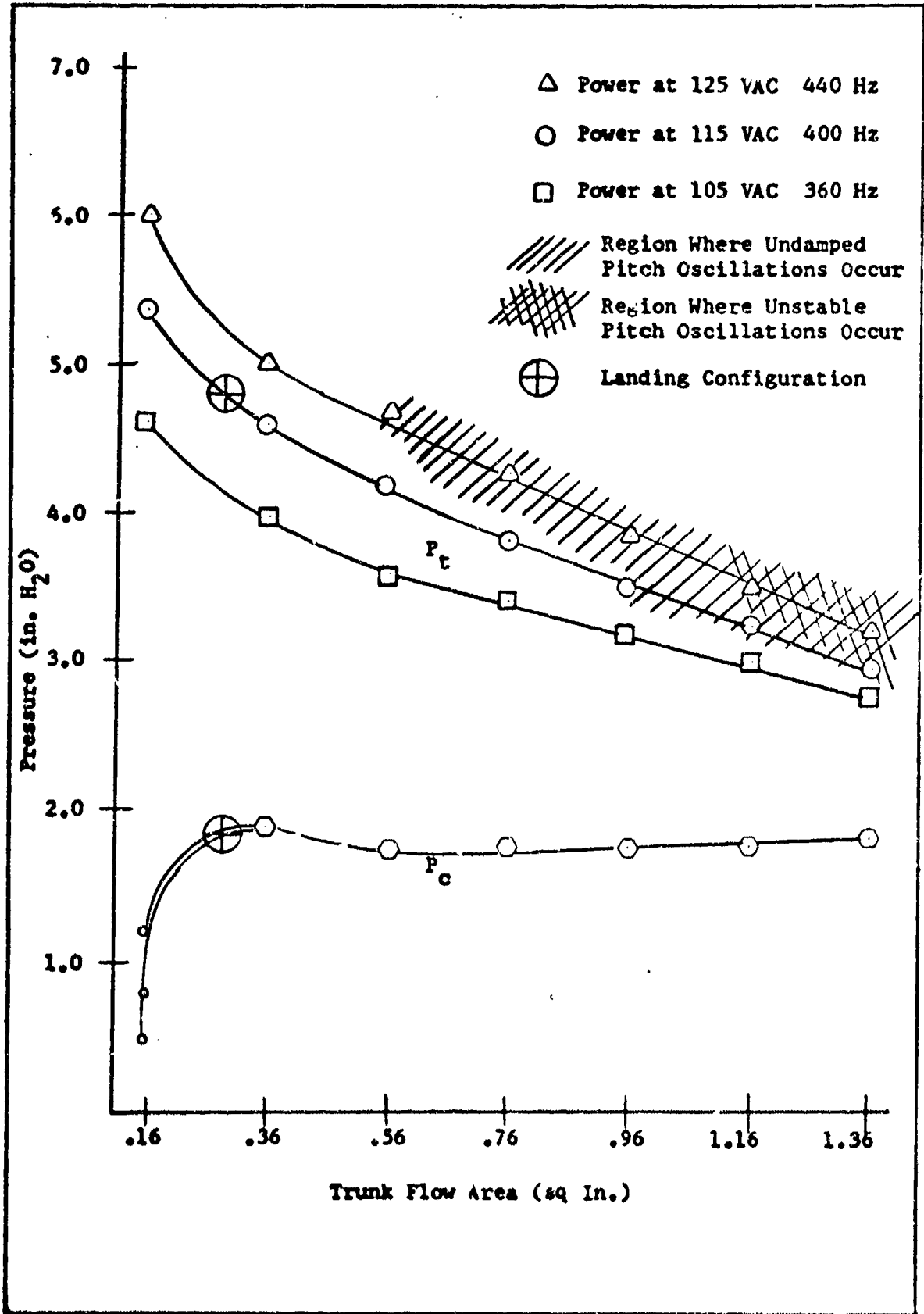


Fig. 5. ACLS Pressure Response to Trunk Flow Area Change

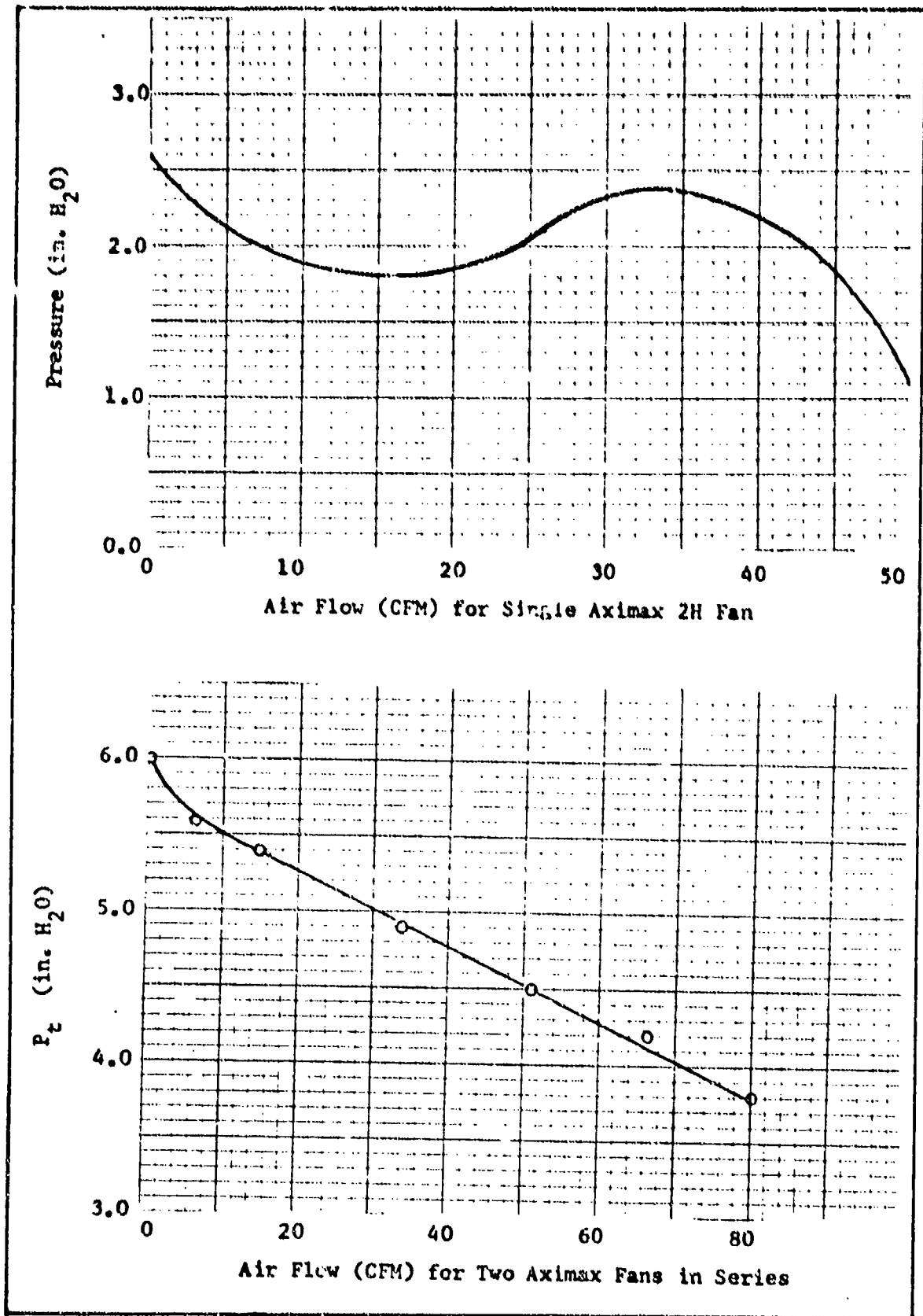


Fig. 6. Performance of Air Supply System

bottom of the trunk, does not occur in drop tests, the cg being aft of the cp causes increased pitch oscillation. It was decided to move the cg directly over the cp for the tenth-scale drop tests and static tests. This was done by placing a weight in the nose of the model which increased the total weight of the model to 2.563 lb. This added weight was removed for the forward speed tests, moving the cg to .6 in. aft of the cp.

Pull Tests

Pull tests were conducted on the tenth-scale model to help check the validity of the landing configuration. It was important in forward speed tests that the pull force F_p required to move the model be properly scaled to the force required to move the full-scale ACLS. The scaled value of the pull force required to move the full-scale vehicle is $.417 \pm .07$ lb. The measured value of F_p for the tenth-scale model in the landing configuration was $.42 \pm .02$ lb. Additional results of the pull tests for the system in different configurations are found in Table VIII of Appendix E.

IV. Static Tests

Static tests were conducted on the tenth-scale ACLS to determine the heave stiffness, roll stiffness and pitch stiffness. Stiffness factors were computed from the data of these tests and compared against full scale test results to determine the degree of similarity in static performance of the two systems. It was found that the agreement in roll stiffness was good but that the tenth-scale ACLS was considerably stiffer in pitch and heave.

Heave Stiffness

The heave stiffness factor K_h is a measure of the amount of vertical displacement of the vehicle as weight on the vehicle is increased. Weight, in 1/4 lb increments, was added to the cg of the model. Measurements were made of the vertical displacement of the wing roots after each increment of weight was added. The displacement of the cg was estimated by averaging the displacement of the wing roots. Previous ACLS model tests have shown the functional relation between deflection vs weight to be quite linear (Ref 2:50-51). The graph of Fig. 7 shows the deflection vs weight relation of the tenth-scale ACLS to be nearly linear. The slope of the curve of Fig. 7 was computed by using the extended difference method and was used as the heave stiffness factor. K_h for the tenth-scale ACLS in the landing configuration was found to be $10.97 \pm 2\%$ lb per in. When converted to the full scale value this becomes $1097 \pm 2\%$ lb per in. and compares with K_h for the full-scale model of $700 \pm 7\%$ lb per in. The greater stiffness of the tenth-scale ACLS is due primarily to the improperly scaled weight and

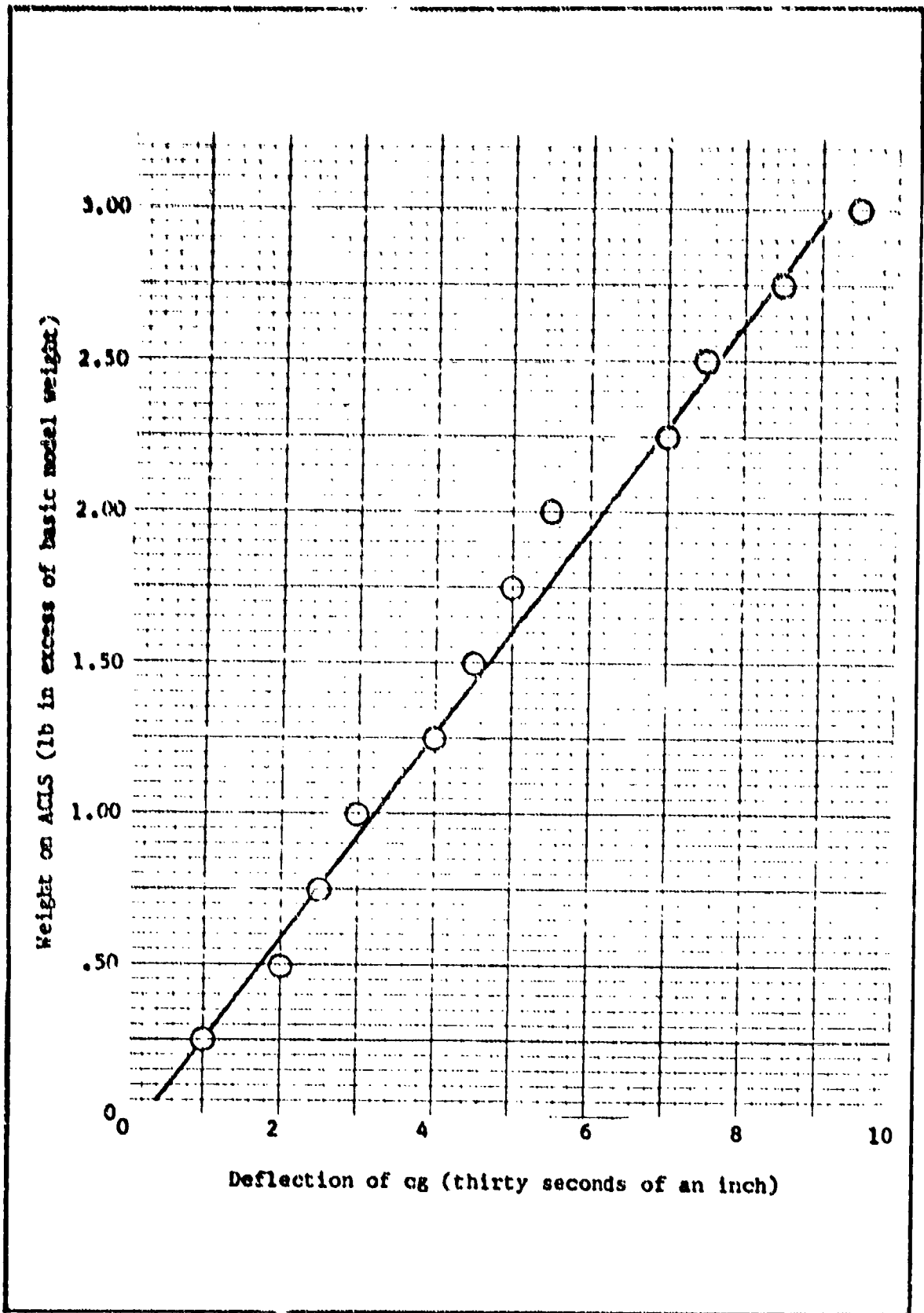


Fig. 7. ACLS Deflection with Load Over the cg for Landing Configuration

thickness of the trunk material. The heave stiffness factor was found to be $8.37 \pm 2\%$ lb per in. for the landing configuration with the air cushion vented. The heave stiffness in the take off configuration was $10.00 \pm 2\%$ lb per in. Figure 14 shows the non linear effects of air leaks around the trunk and the elasticity of the trunk cause the weight vs deflection relation to become non linear as the weight added to the cg becomes larger than 3 lb. K_h for the cushion vented take off configuration had two values. Over the range where trunk pressure increased as weight was added the stiffness was $12.8 \pm 2\%$ lb per in. After P_c reached a maximum value of 5.45 in. H_2O stiffness became $6.4 \pm 2\%$ lb per in. The change in the value of K_h is shown in Fig. 15 by the definite change in slope at a load of 1.7 lb. The data for these tests are tabulated in Appendix E.

Pitch Stiffness

The pitch stiffness factor K_θ is a measure of the change in pitch attitude caused by a torque being applied about the center of gravity in the pitching plane. The necessary information for computation of the pitch stiffness factor was obtained by applying a torque about the lateral axis (pitching moment) and determining the angular change in pitch attitude of the model. The torque was applied by placing a weight on the nose or tail of the model and removing an equal amount of weight from the cg of the model. The angular deflection was computed from measurements of the change in height of the tip of the nose and base of the tail. (See Appendix F for details on the necessary computations.) The deflection angle vs weight added relation was found to be linear as shown in Fig. 8. Using the extended difference method, the slope of the

deflection angle vs weight added curve was computed and multiplied by the moment arm to find the stiffness factor. K_{θ} for nose down moment (negative pitch moment) was found to be $.155 \pm 3\%$ lb ft per deg. The value of K_{θ} for a positive pitch moment was found to be $.130 \pm 3\%$ lb ft per deg. These values when converted to full-scale are $1550 \pm 3\%$ lb ft per deg and $1300 \pm 3\%$ lb ft per deg. They are considerably higher than the value of the pitch stiffness for nose down moment determined from full-scale tests of $900 \pm 6\%$ lb ft per deg.

Roll Stiffness

The roll stiffness is a measure of the amount of roll caused by a torque being applied about the cg in the roll plane. The value of the roll stiffness factor K_{ϕ} was determined by comparing the change in roll angle with torque applied about the longitudinal axis. The torque was applied by adding weight to a wing tip while taking an equal amount of weight off the cg. The change in bank angle was determined from measurements of the change in height of each wing tip after the weight was applied. As shown in Fig. 9 the relation of roll angle to weight added was linear. The same method used in computing the pitch stiffness factor was used to find the roll stiffness factor. K_{ϕ} for a positive rolling moment (weights on the right wing) was $.00493 \pm 3\%$ lb ft per deg, and for a negative moment was $.00466 \pm 3\%$ lb ft per deg. When converted to full-scale, these values became $49.3 \pm 3\%$ lb ft per deg and $46.6 \pm 3\%$ lb ft per deg. The tenth-scale values of K_{ϕ} show good agreement with the full-scale ACLS value of $60 \pm 6\%$ lb ft per deg.

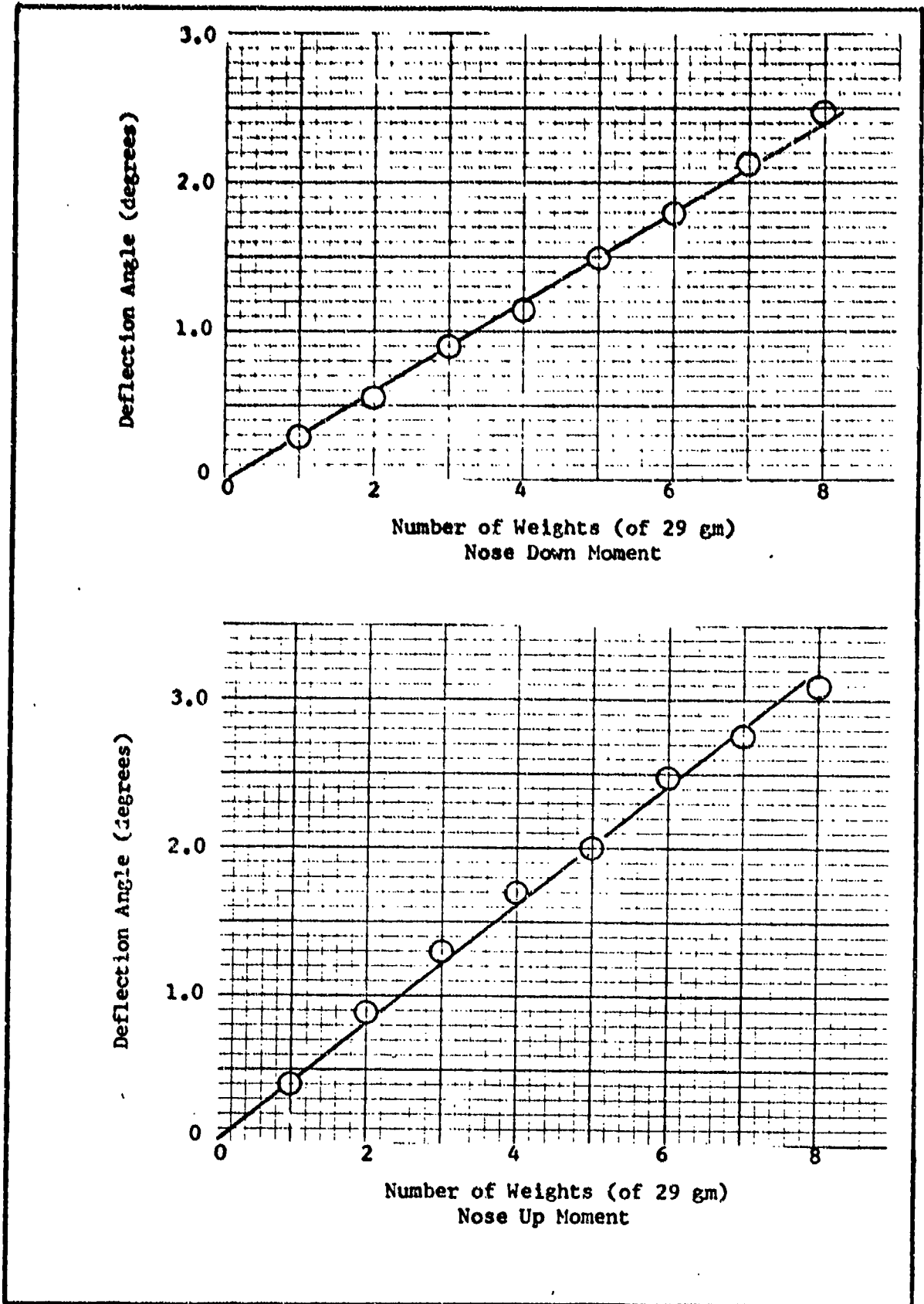


Fig. 8. Effect of Pitching Moment on ACLS Pitch Attitude

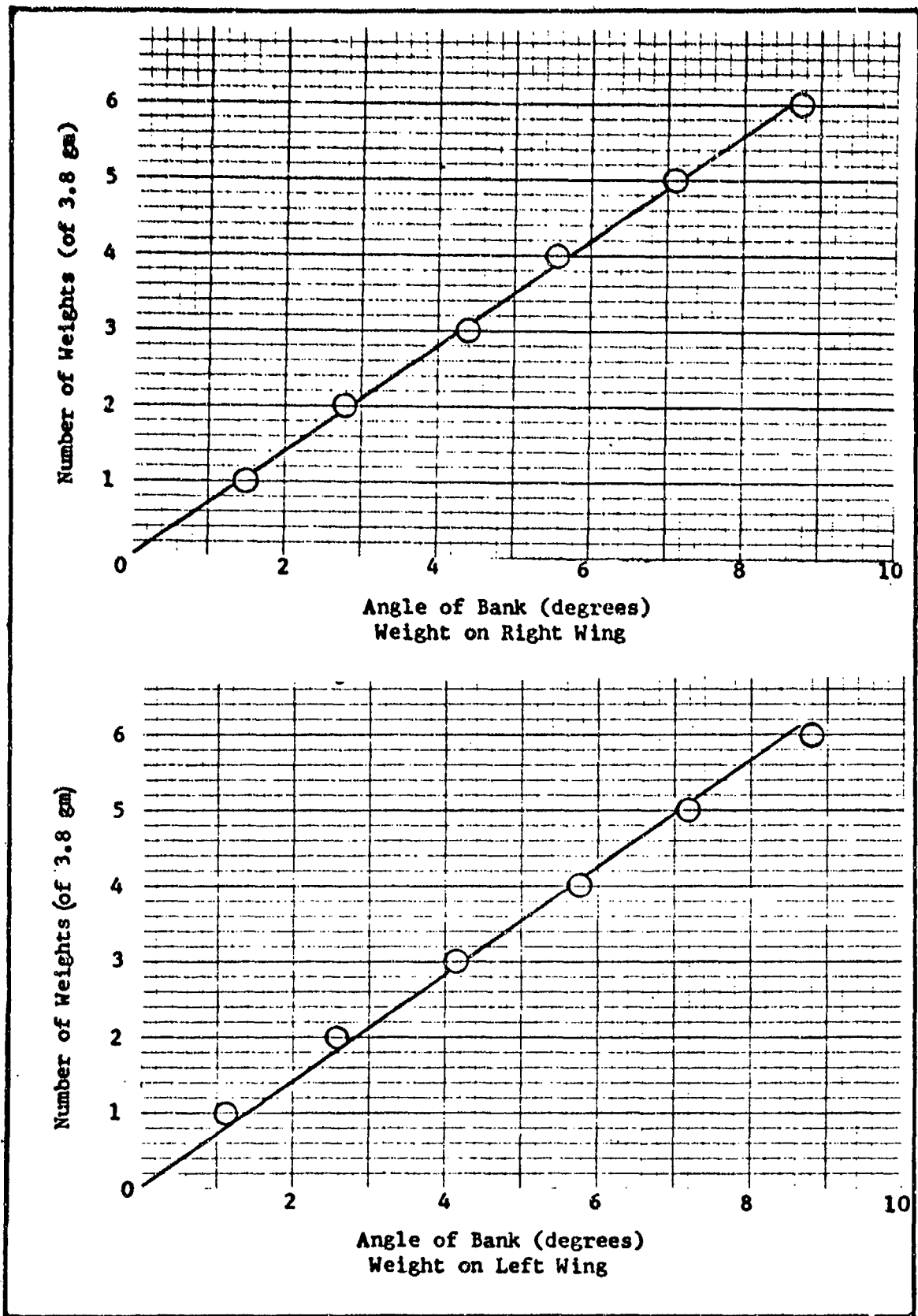


Fig. 9. Effect of Rolling Moment on ACLS Bank Angle

V. Drop Tests

Drop tests were conducted to determine the dynamic response of the tenth-scale ACLS to the vertical forces of landing. Trunk pressure, cushion pressure and acceleration of the cg a_{cg} were measured as the tenth-scale model was dropped from specified heights. The tests were conducted from release heights of 1.0 in., 2½ in. and 3½ in. These selected drop heights yield vertical velocities similar to full-scale descent rates of 7.5 fps, the nominal landing descent rate, 11 fps and 14 fps, the maximum landing descent rate.

Instrumentation

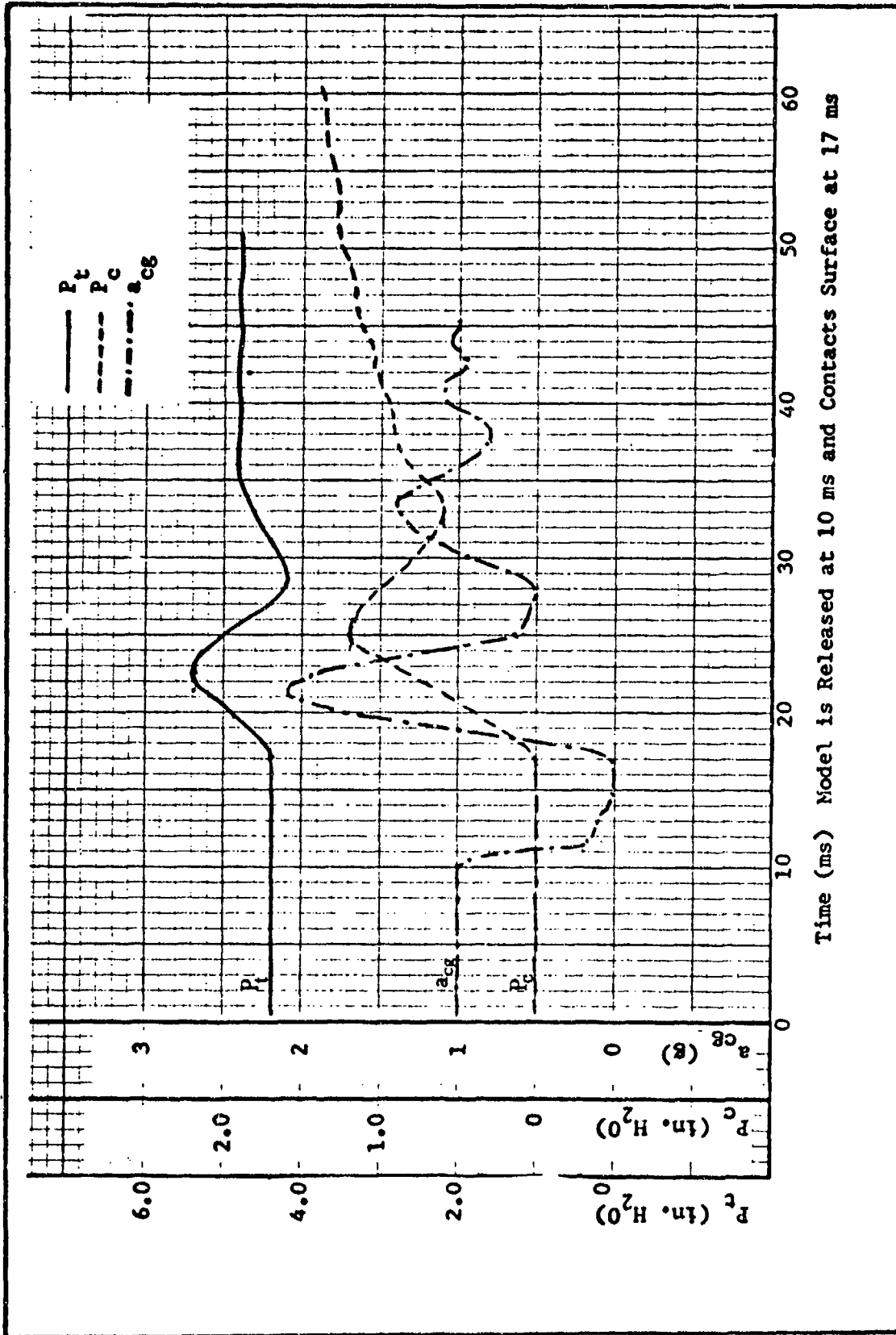
Pressure measurements were taken with strain gage type pressure transducers from pressure taps located in the trunk region and cushion region. The acceleration was measured by a strain gage type accelerometer located 2 in. aft of the cg. The signals were displayed on an oscillograph by a Visacorder. A light-weight piezoelectric accelerometer was used in some of the tests but the output was less satisfactory as explained in Appendix D. The pressure transducers were calibrated before each drop by comparing the static IGE reading of the trunk and cushion pressures with water manometers reading the same values. The accelerometer could be checked for each test by comparing the deflection prior to release (1 g) with that immediately after release.

Results of Drop Tests

It was found that the acceleration forces measured in the tenth-scale drop tests showed good agreement with measurements taken in the

full-scale tests. The pressure response showed little correlation with full-scale data. When converted to full scale readings, the peak trunk pressure for landings at nominal descent rate is 1.95 psig. This compares to a value for the full-scale tests of 2.5 psig. The converted value of the peak cushion pressure for the tenth-scale ACLS was .35 psig. This compares with 1.2 psig for the full-scale ACLS under similar conditions. The primary reason for lack of agreement between the systems is the difference in air supply systems. The full-scale system employs a centrifugal flow fan which has good backflow/recovery characteristics while the tenth-scale model uses two axial flow fans in series, a system with poor backflow/recovery characteristics. Neither pressure appeared to vary in phase with a_{cg} ; instead, trunk pressure quickly reached a steady state value while cushion pressure rose slowly to the value for static hover. (See Fig. 10.)

Comparison in the loading at the cg of the two Jindivik models show them to be similar in this area. The peak load on the cg of the tenth-scale ACLS for the nominal descent rate landing was 2.2 g's. The value recorded in full-scale tests was 2.3 g's. The tenth-scale values for peak a_{cg} recorded in tests with the cushion vented were essentially the same as the values recorded with the vent closed. This indicates that the air cushion had little effect upon the peak g of landing. This observation was also made from drop tests of the full-scale ACLS. It was found for the tenth-scale system that at the nominal descent rate, the peak g forces were significantly less for drop tests conducted with no air flow to the system (1.65 g vs 2.2 g). This may indicate that a stiffer trunk with less air flow may be a better energy absorption system. Tables XI and XII summarize the results of the drop tests.



Time (ms) Model is Released at 10 ms and Contacts Surface at 17 ms

Fig. 10. Sample Drop Test Schematic

VI. Catapult Tests

Catapult tests were conducted to simulate the dynamics of a landing. High speed films were made of the tests showing the effects of catapult separation and touchdown upon the model. The tests were conducted at representative speeds throughout the range of catapult operation.

Launch Velocity

The launch velocity of the model was calculated for a number of launching conditions. The full travel of the carriage was measured and timed. These values were used to calculate the acceleration of the carriage. The launch velocity V_L of the model was then computed for different carriage release points along the catapult rails. Appendix F shows the details of these calculations.

The catapult tests were conducted at launch velocities of 11.4 fps, 18.7 fps, 26.4 fps and 30.5 fps (velocities are accurate to $\pm 10\%$). The final velocity represents the maximum attainable velocity for the catapult configuration used in these tests.

Separation From the Catapult Carriage

It was determined from the high speed film that the catapult/model separation was flawless throughout most of the operating speed range but that at the maximum attainable speed the carriage pitched forward after hitting the stop causing the front carriage support to strike the rear launch mount of the model as it passed underneath. The subsequent pitch-up of the nose of the model caused the model to touch down with a nose high pitch angle of approximately 10 deg.

Configuration

The model was configured as closely as possible to the full-scale Jindivik in the landing configuration. The weight placed in the nose of the model during static and drop tests was removed, moving the cg to $.6 \pm 20\%$ in. aft of the cp. It was desired to evaluate the pitch response of the model at two configurations. The normal landing configuration was to be compared to the high-drag configuration achieved with the air cushion vented. The proper positioning of the aircraft cg and proper balance of drag moment and air cushion moment are critical at touchdown. If the force created by P_C acting over A_C is large and if the cg is too far from the cp, a nose up pitching moment will result which can cause the vehicle to pitch up after landing and become air-born in a near stalled attitude. On the other hand if the moment due to drag is large compared to that caused by $P_C A_C$, the nose will pitch down on landing which is also undesirable. The drag and air cushion moments about the cg for the two configurations are shown in Fig. 11.

It was determined from the high speed films that at 11.4 fps and 18.7 fps, the model tended to pitch up after touchdown in the normal landing configuration. At the same speeds with the air cushion vented, the model maintained a level pitch attitude after touchdown. The results of launches at higher speeds were inconclusive because of the narrow field of view of the high speed camera.

Braking Coefficient

Measurements were made of the slide out distance for the different launch speeds and configurations. The estimated touchdown speed and slide distance were used to compute the deceleration during slide out.

An average braking factor was then computed for the cushion vented configuration. The value thus computed for the tenth-scale braking factor was $.33 \pm 20\%$ which compares with the full-scale value of $.35$. Appendix F shows the details of the above calculations.

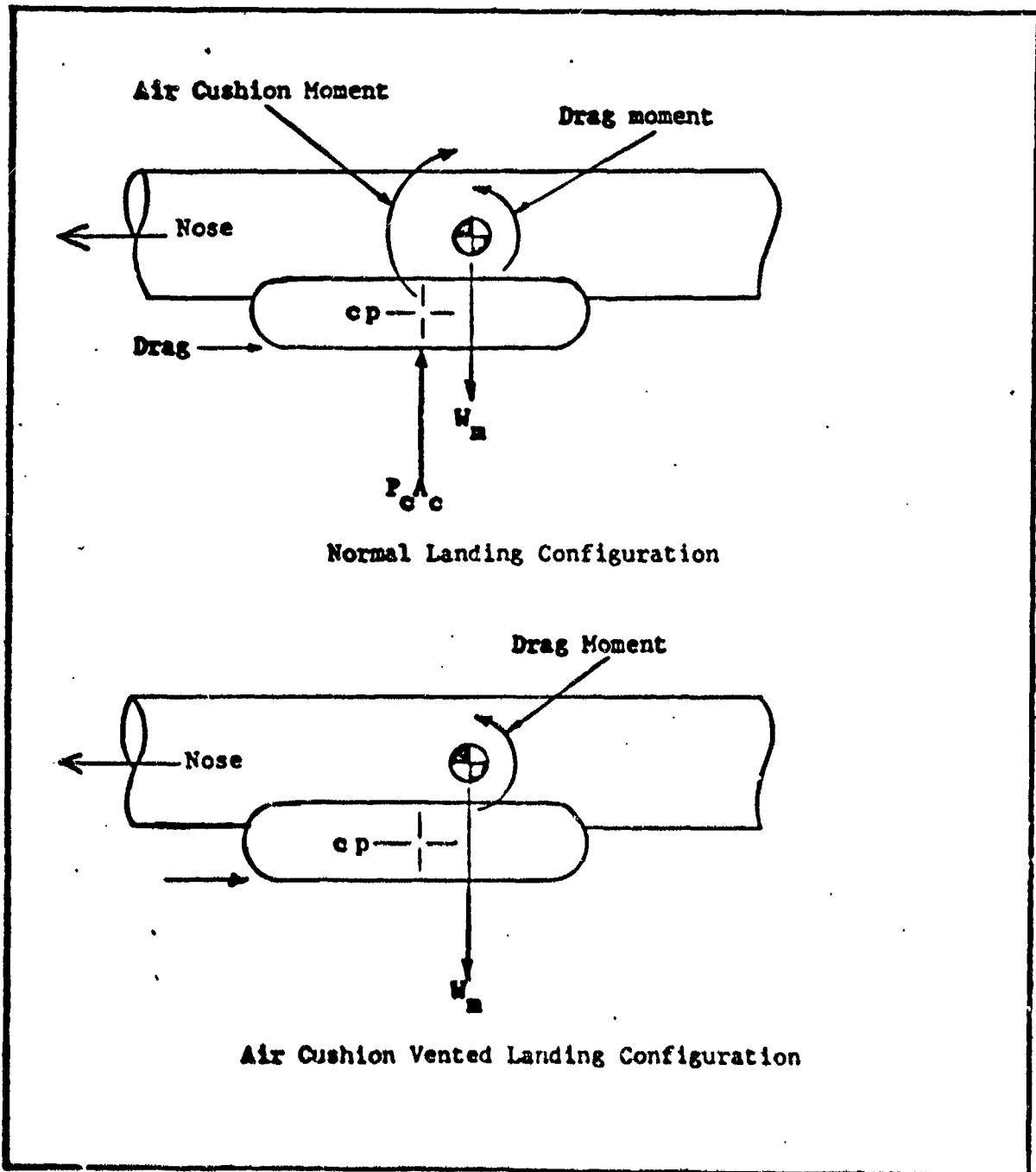


Fig. 11. Adverse Pitch Moments at Touchdown

VII. Conclusions and Recommendations

Conclusions

An experimental investigation of the performance of an ACLS installed on a tenth-scale model Jindivik RPV has been conducted. The results of this investigation have been compared to similar results from tests performed on an ACLS installed on a full-scale model Jindivik. Based on experimental results and comparison to full-scale test results, the following conclusions are drawn:

1. The dynamic load at the center of gravity, resulting from drop tests, was similar for the two systems. This conclusion is drawn from results of similar drop tests conducted on the tenth-scale and full-scale systems. At the nominal descent rate for landing, the peak acceleration force at the cg of the tenth-scale system was 2.2 g's compared to 2.3 g's for the full-scale system. The results for both systems, of tests conducted at a particular air flow and trunk flow area, showed that the peak load at the cg was the same for the air cushion vented configuration as for the normal landing configuration.

2. The response of trunk and cushion pressure of the tenth-scale system, to the dynamics of drop tests, did not correlate to the pressure response of the full-scale system. The peak cushion pressure for tenth-scale tests at the nominal descent rate converted to a full-scale reading was $.28 \pm 10\%$ psi. The value of P_c recorded in a similar full-scale test was $1.2 \pm 10\%$. The rise time for the tenth-scale P_c to reach its equilibrium value was an order of magnitude greater than the comparable full-scale value.

3. High speed films of catapult tests showed that for touchdown speeds up to 12 mph (at the nominal descent rate) the aircraft pitch oscillations which occurred after touchdown were significantly smaller when the model was landed with the air cushion vented compared to landings in the normal landing configuration.

4. The positive or nose down pitch stiffness of the tenth-scale ACLS was 19% higher than the negative pitch stiffness value of .13 lb ft per deg. The roll stiffness of $.0048 \pm 3\%$ lb ft per deg was too low to operate the model in taxi and landing tests without a wing tip contacting the ground.

5. The tenth-scale Jindivik ACLS did not accurately predict the stiffness of the full-scale system, but a reasonable order-of-magnitude approximation of full-scale stiffness was obtained. A comparison of the scaled stiffness factors of the tenth-scale ACLS with the same values for the full-scale system show the tenth-scale ACLS to have greater pitch stiffness ($1550 \pm 3\%$ lb ft per deg vs. $900 \pm 6\%$ lb ft per deg) and greater heave stiffness ($1100 \pm 2\%$ lb per in. vs. $700 \pm 7\%$ lb per in.) and less roll stiffness ($48 \pm 3\%$ lb ft per deg vs. $60 \pm 6\%$ lb ft per deg).

Recommendations

Based on findings of this experimental study and on unexplained observations recorded in experiments conducted in support of this study, the following recommendations are made:

1. An improved method should be developed for the attachment of the small scale ACLS trunk to the model. The attachment system should minimize leaks around the trunk attachment line and eliminate the added stiffness caused by the tape and caulk used to prevent these leaks. The

system should be designed to facilitate the removal and replacement of the trunk so that a variety of trunk designs may be tested.

2. The undamped and unstable pitch oscillations which occurred in a significant region of the tenth-scale ACLS operation should be examined experimentally or analytically to explain the occurrence and predict conditions where unstable operation may occur in other air cushion landing systems.

3. The catapult tests should be repeated using a heavier drop weight and a longer landing zone. High speed camera coverage should be increased to include more of the landing dynamics. The forward pitching of the carriage at high speeds can be diminished by redesigning the carriage stop.

4. The possibility of using a battery to power the ACLS air supply system should be investigated. A battery powered system would eliminate the extraneous forces caused by the power umbilical.

Bibliography

1. Air Force Flight Dynamics Laboratory. Unpublished notes on Ground Tests of an Air Cushion Recovery System of a Drone Aircraft. Vaughan, John C., III, Chief Scientist; Steiger, J. T.; Campbell, S.; Pool, D. J. June - October 1973.
2. Rodrigues, Anthony. Drop and Static Tests on a Tenth-Scale Model of an Air Cushion Landing System. Unpublished Thesis. Wright Patterson Air Force Base, Ohio; Air Force Institute of Technology, March 1973.
3. Rotron Mfg. Co., Inc. Brochure on the Aximax 2 Vaneaxial Fan. 3-63-12m. Rotron Mfg. Co., Inc., Woodstock, New York. 1958.

Appendix A

Scale Verification

Scaling parameter determination was based on a constant Froude number for the flow beneath the ACLS, a constant density and constant linear acceleration between systems. These constraints were used in computing scale factors for the properties of interest. Table I gives a summary of these properties, their scale factors and the full-scale and desired tenth-scale values for the Jindivik RPV. The conversion factors are computed using definitions, dimensional analysis and the basic equation $F = ma$.

Table I
Scaled Values for Tenth-Scale Jindivik Design

Quantity	Units	Symbol	Full-Scale	Scale ^a Factor	Tenth-Scale
Trunk Pressure	psig	P_t	1.7	S	.17
Cushion Pressure	psig	P_c	.61	S	.061
Force	lb_f	F	--	S^3	--
Time	sec	t	--	$S^{1/2}$	--
Density	lb_m/ft^3		.0825	1	.0825
Nominal Descent Rate	ft/sec	V_v	7.66	$S^{1/2}$	2.43
Landing Weight	lb_f	W_m	2700	S^3	2.7
Length	ft	L	23.31	S	2.33
Span	ft	b	20.75	S	2.075
Cushion Area	in^2	A_c	2346	S^2	23.46
Max Structure Load	g	g_{max}	5	1	5

a For tenth-scale, scale factor $S = 1/10$

Appendix B

Small Scale ACLS Trunk Manufacture

Previous ACLS trunks have been made from a rubberized fabric cut in a pattern and sewn together to form the trunk. The inside radius of the tenth-scale Jindivik trunk as shown in Fig. 12 is .3 in. The cross section of the trunk has two radii of curvature and a section in contact with the fuselage. The toroidal shape of the trunk, the complex cross section and the small inside radius at the ends of the toroid made it difficult to fashion a pattern out of a flat piece of fabric and a nightmare to make the pattern into a trunk. For this reason a new technique was developed to make the trunk. A positive mold of the trunk was made of wood. The mold was covered with a mixture of talcum powder in wood alcohol and then dipped for two minutes in a vat of liquid latex rubber. The thickness of the latex rubber can be varied by repeated dippings or by changing the length of time the mold is dipped. The trunk was dipped in a liquid coagulant and hung up to dry. After drying the trunk was cured by baking it for 1 hr in a kiln at 225 F. A seam was cut around that portion of the trunk which would be against the model fuselage and the mold was removed. The desired hole pattern was cut in the trunk then it was taped together and fastened to the fuselage by two way tape. The interior of the trunk, along the line where it contacted the fuselage, was calked and taped to prevent air from escaping from the trunk into the cushion region. The trunk was then ready for testing.

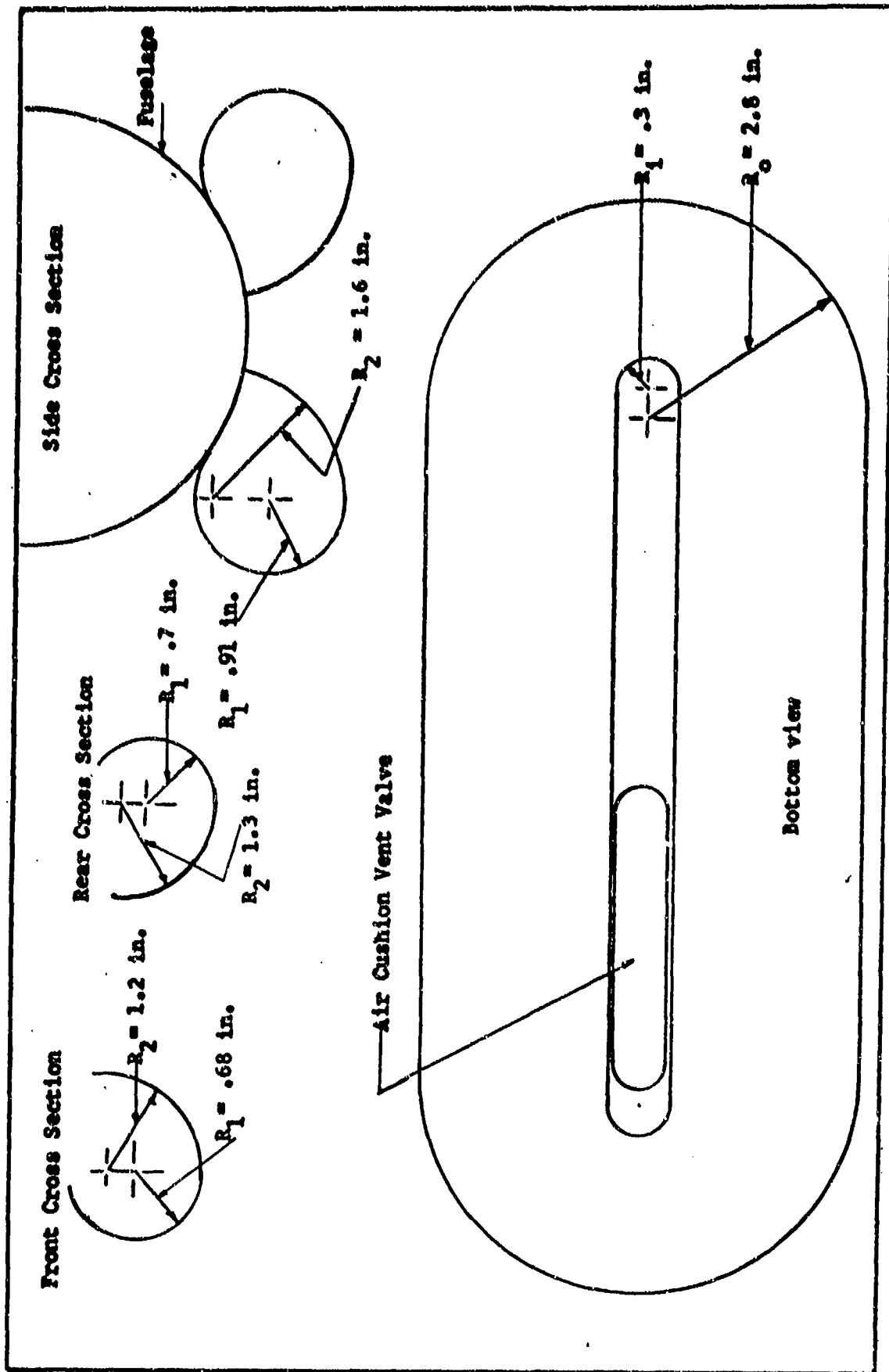


FIG. 12. ACLS Trunk

Appendix C

Catapult Design

A catapult was designed to launch the model for landing tests. The catapult used a weight and pulley system to accelerate the model. The constraints imposed upon the design were that the maximum drop height for the weight was 14 ft, the area available for catapult installation and landing zone was 90 ft long and the materials available for the catapult launch rails were two 25 ft aluminum channel beams.

In trying to get the highest launch speed, systems having a mechanical advantage of 1, 2 and 4 were compared using a nominal drop weight of 50 lb and a catapult length of 24 ft. Using the principle of conservation of energy it was determined that the best system was the one with the mechanical advantage of 2. The equation used in the calculations sets the maximum potential energy of the drop weight equal to the kinetic energy at launch of the drop weight plus the carriage and model. The launch velocity is solved for from the above relation.

The front and rear catapult supports are height adjustable allowing the release altitude and the launch velocity vector to be varied. The front and rear model supports on the catapult carriage are also height adjustable which allows the pitch attitude of the model at release to be varied.

Appendix D

Instrumentation

The testing of a small scale model required that the instrumentation provide good resolution with a minimal amount of loading on the system. The problems encountered in instrumentation were primarily due to the fact that sophisticated instruments providing the desired resolution were too large, too complex or too expensive. For most of the tests, a simple test set up employing inexpensive, easy to use, readily available measurement apparatus was found to be satisfactory.

ACLS Operating Characteristics: The diameter of the ports in the trunk which provided air flow to the cushion were measured with an engineers scale to an accuracy of $\pm .02$ in. The gage pressure was measured with a U-tube water manometer to an accuracy of $\pm .025$ in. H_2O .

Static Stiffness Determination: The weights used to provide the moment on the ACLS for pitch and roll stiffness tests were weighed to an accuracy of $\pm .5$ gm. The weights used to load the cg in the heave stiffness test were measured to an accuracy of ± 2 gm. These weight measurements were made with a two arm balance scale with a resolution and accuracy of .1 gm. The moment arms were measured to an accuracy of $\pm .25$ in. The deflections of the model were measured to the nearest 32nd of an inch. Trunk and cushion pressures were measured with U-tube manometers which provided gage pressure readings accurate to $\pm .025$ in. H_2O .

Drop Test Measurements: The drop tests involved dynamic measurements of pressure response and g loads. The instruments used in these tests

were necessarily more sophisticated. The trunk and cushion pressures were measured by Bell and Howell type 4-312-0050 pressure transducers. These transducers had a range of ± 2.5 psi and a sensitivity of ± 500 mv per psi. The acceleration of the cg was measured by one of two instruments. The most satisfactory in terms of output was a Bell and Howell type 4-202-0001 accelerometer with a range of ± 10 g and a sensitivity of 4.6 mv per g. This accelerometer weighed 80 gm and was located 2 in. aft of the cg. In this position it provided more loading on the system than was desired. The combined nonlinearity and hysteresis error for the pressure transducers was .15% of full range and for the accelerometer was .11% of full range. The BBN 501 accelerometer weighed 1.8 gm and, located 2 in. aft of the cg, provided a negligible load on the system. This piezoelectric accelerometer measured only the dynamic g's and during short periods of equilibrium such as during free fall, the signal from the BBN 501 would decay exponentially. With large accelerations such as the 3 to 5 g signal due to a landing, the zero of the BBN 501 tended to drift. For these reasons, only the initial peak g forces of a landing could be satisfactorily measured. By comparing the peak g signal of the BBN 501 with that of the Bell and Howell accelerometer for similar tests, it was determined that an accuracy of $\pm 10\%$ could be expected in the peak g signal of the BBN 501.

The signals from the pressure transducers and Bell and Howell accelerometer were fed to Bell and Howell type 8-114 signal conditioners. These conditioners provided the necessary excitation voltage to the instruments, the variable gain provided the desired output level and the filtering system cut out noise with frequencies of 30 cps and greater.

The BBN 501 signal was amplified by a Dymec Model 2460A amplifier. The conditioned signals went to Honeywell M-100-350 galvanometers. These galvanometers had a sensitivity of 2.32 in. per mv with flat response to an input frequency of up to 60 cps. The galvanometer output was linear to within $\pm 2\%$ for a peak to peak output range of 8 in. The output signals of the galvanometers were displayed by a Honeywell Visacorder. The oscillograph could be read to an accuracy of $\pm .05$ in. This corresponded to values for the signals of $\pm .1$ in. H_2O for trunk pressure, $\pm .05$ in. H_2O for cushion pressure and $\pm .05$ g for the load at the cg.

Catapult Tests: The tests were filmed with a high speed camera at a rate of 250 frames per sec. The launches at V_L max were filmed at 500 frames per sec. The slide out distance was measured to an accuracy of $\pm 4\%$.

Pull Tests: The device used to measure F_p was a spring deflection type gage with a resolution of .01 lb. This gage was calibrated and found to be accurate to $\pm .01$ lb and linear throughout its range of measurement. This gage was fixed to the model by means of a pulley system with a weight counterbalancing the gage weight. F_p was determined by subtracting the force required to raise the counterbalance weight from the force measured to pull the model. In the cases where F_p was greater than 1 lb the counterbalance weight was not used and the weight of the gage was added to the measurement force to determine F_p . The system was deemed accurate to $\pm .02$ lb at values of F_p below 1 lb, and to $\pm .05$ lb for F_p above 1 lb.

Appendix E

Summary of Test Data

The data taken in the tests performed in support of this study are summarized in the figures and tables of this appendix.

Air Supply System Performance with Changing Flow Rate: The air supply system was tested to determine the pressure rise created by the two axial flow fans in relation to the flow rate of the system. The flow rate is dependent upon the pressure rise across the fans and upon the flow area downstream of the fans. It was assumed that P_t was equal to the pressure rise of the system. P_t was measured OGE as the trunk flow area was varied and the flow rate was computed as shown in Appendix F. Table II contains the data of this test.

Determination of ACLS Pressure Response to a Change in Trunk Flow Area: As discussed in Chap. 3 the trunk and cushion pressures and the pitch stability of the ACLS were checked for a number of flow areas at different power settings. Table III gives the data from this test.

Pull Test: The force required to pull the model forward at a slow speed was measured for a number of configurations. The results are tabulated in table VIII.

Heave Stiffness Test: Lead shot bags were placed over the cg of the model and the change in the height of the wing roots was measured as were the trunk and cushion pressures. From the data an average deflection per unit weight was computed and used as the heave stiffness factor. Tests were conducted at a number of different configurations representing the normal landing configuration, the cushion vented landing configuration, a take off configuration and an air cushion

vented take off configuration. Tables IV -VII give the results.

Roll Stiffness Test: A torque about the longitudinal axis was applied by placing weights on the wing. The distance from each wingtip to the surface was measured for each torque applied. The angular deflection about the longitudinal axis was computed and the average angular deflection per unit torque was used as the roll stiffness factor. The data from the roll stiffness tests are found in tables IXa and IXb.

Pitch Stiffness Test: A torque about the lateral axis was applied by placing weights on the nose or tail of the model. The distance between the surface and the tip of the nose and the base of the tail was measured for each torque applied. The angular deflection about the lateral axis was computed and the average angular deflection per unit torque was used as the pitch stiffness factor. The data from the pitch stiffness tests are tabulated in tables Xa and Xb.

Drop Tests: Drop tests were conducted to determine the ACLS pressure response and peak loads imposed upon the cg by the vertical forces of landing. The tests were conducted from different drop heights in a number of configurations. Table XI and XII summarize the data taken in the drop tests.

Braking Factor: The model's slide out distance for the catapult tests provided information on the sliding friction coefficient. A braking factor was computed for the air cushion vented landing configuration. As a check for the computed braking factor the cushion area was computed using the average braking factor of Table XIII and a nominal cushion pressure of 1.0 in. H_2O . The theoretical value was compared to the estimated value of the static A_c . The results are shown in Table XIV.

Table II

Trunk Pressure and Flow Rate vs Trunk Flow Area

Effective Trunk Flow Area $C_d A_n$ (in. ²)	Power Frequency (HZ) / Voltage (VAC)	Trunk ^a Pressure (in. H ₂ O)	Flow Rate (cfm)
All ports closed	360/105	5.2	0
	400/115	6.0	0
	440/125	6.8	0
.0035	360/105	5.0	2.13
	400/115	5.8	2.31
	440/125	6.6	2.44
.007	360/105	4.90	4.22
	400/115	5.75	4.56
	440/125	6.40	4.84
.0105	360/105	4.80	6.28
	400/115	5.65	6.80
	440/125	6.30	7.17
.014	360/105	4.80	8.37
	400/115	5.60	9.03
	440/125	6.25	9.53
.0165	360/105	4.60	14.6
	400/115	5.40	15.8
	440/125	6.20	16.9
.0255	360/105	4.25	33.8
	400/115	4.90	36.3
	440/125	5.70	39.2
.0605	360/105	3.90	51.3
	400/115	4.50	55.0
	440/125	5.20	59.2
.0954	360/105	3.55	66.7
	400/115	4.20	76.3
	440/125	4.80	77.7
.1304	360/105	3.20	80.6
	400/115	3.80	87.8
	440/125	4.35	93.8

^aMeasurements taken out of ground effect.

Table III

ACLS Pressure Response as a Function of Trunk Flow Area

Trunk Flow Area A_n (sq in)	Power Frequency (HZ)/ Voltage (VAC)	Stability ^a	Trunk Pressure (in. H ₂ O)	Cushion Pressure (in. H ₂ O)
.16	360/105	S	4.60	.50
	400/115	S	5.40	.80
	440/125	S	6.00	1.20
.36	360/105	S	4.00	1.85
	400/115	S	4.60	1.90
	440/125	S	5.00	1.90
.56	360/105	S	3.60	1.80
	400/115	S	4.20	1.75
	440/125	N	4.70	1.70
.76	360/105	S	3.40	1.80
	400/115	S	3.80	1.80
	440/125	N	4.30	1.75
.96	360/105	S	3.20	1.80
	400/115	N	3.50	1.75
	440/125	N	3.85	1.80
1.16	360/105	S	3.00	1.80
	400/115	N	3.26	1.80
	440/125	U	3.54	1.80
1.36	360/105	S	2.80	1.80
	400/115	U	3.00	1.80
	440/125	U	3.20	1.90

^aPitch stability was tested by observing the response to a pulse applied to the tail. S indicates the oscillations damped to zero, N indicates the oscillations were undamped and U indicates the oscillations were unstable.

Table IV

Deflection of cg with Increased Load for Landing Configuration

Weight (lb)	ΔH_{cg} ^a (32nds in.)	Total ΔH_{cg} (32nds in.)	Cushion Pressure (in. H ₂ O)	Trunk Pressure (in. H ₂ O)
0	0	0	1.85	4.75
1/4	1	1	1.95	4.75
1/2	1	2	2.05	4.75
3/4	.5	2.5	2.20	4.75
1	.5	3	2.30	4.75
1 1/4	1	4	2.45	4.75
1 1/2	.5	4.5	2.55	4.75
1 3/4		5	2.75	4.75
2	.5	5.5	2.90	4.75
2 1/4	1.5	7	2.95	4.85
2 1/2	.5	7.5	3.05	4.90
2 3/4	1	8.5	3.15	4.90
3	1	9.5	3.30	4.90

^a ΔH_{cg} is the vertical deflection of the cg due to increased weight accurate to $\pm 10\%$.

Table V

Deflection of cg with Increased Load for Landing Configuration
with Air Cushion Vented

Weight (lb)	ΔH_{cg}^a (32nds in.)	Total ΔH_{cg} (32nds in.)	Trunk Pressure (in. H ₂ O)
0	0	0	4.70
1/4	3	3	4.75
1/2	1	4	4.80
3/4	.5	4.5	4.95
1	.5	5	5.00
1 1/4	2	7	5.10
1 1/2	0	7	5.20
1 3/4	.5	7.5	5.25
2	.5	8	5.25
2 1/4	2	10	5.25
2 1/2	1	11	5.25
3	2	13	5.25
3 1/2	3	16	5.25
4	3	19	5.25

^a ΔH_{cg} is the vertical deflection of the cg due to increased weight, accurate to $\pm 10\%$.

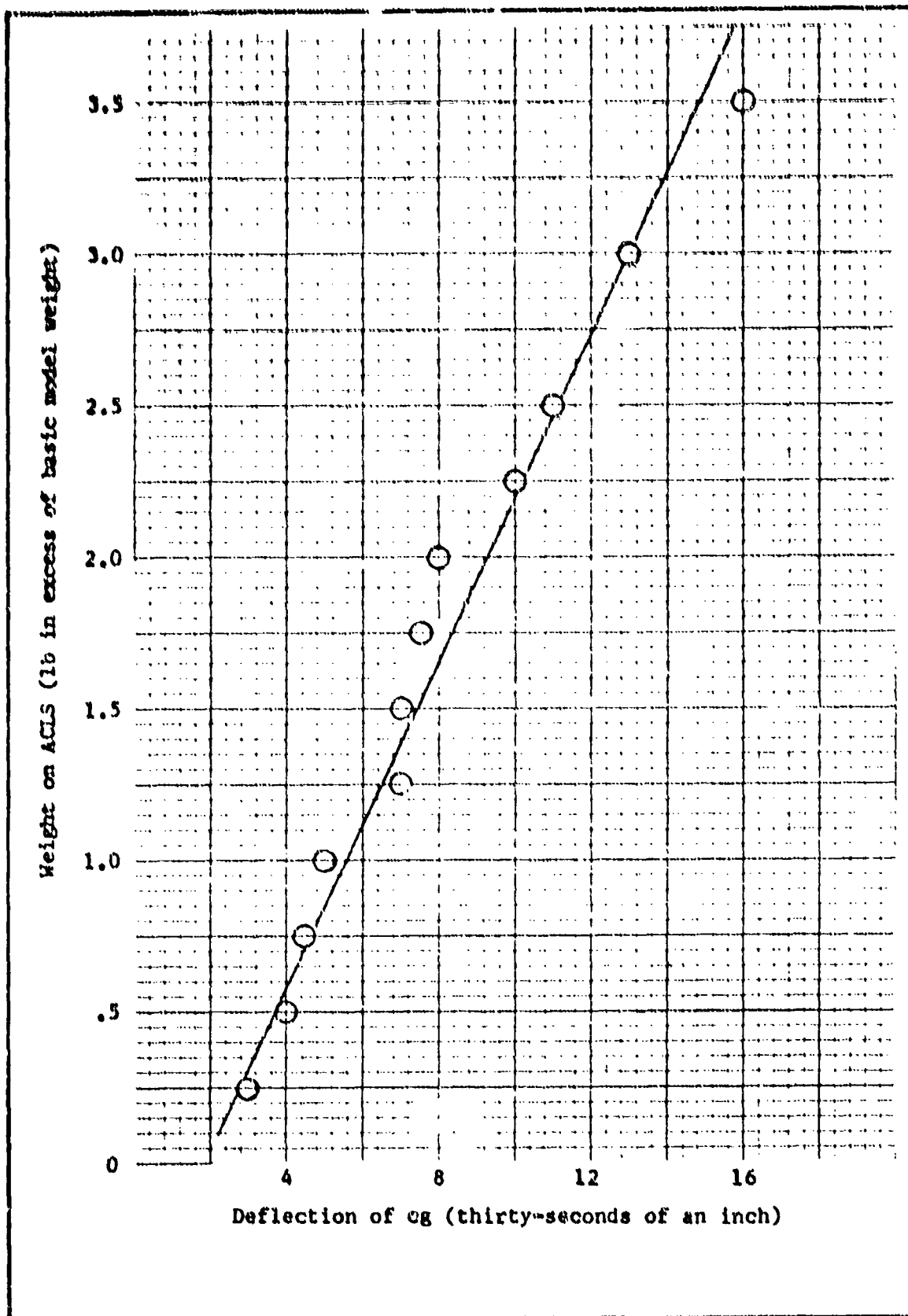


Fig. 13. Deflection of ACLS with Load for Cushion Vented Landing Config.

Table VI

Deflection of cg with Increased Load for Take Off Configuration

Weight (lb)	ΔH_{cg}^a (32nds in.)	Total ΔH_{cg} (32nds in.)	Trunk Pressure (in. H ₂ O)	Cushion Pressure (in. H ₂ O)
0	0	0	3.10	1.90
1/4	.5	.5	3.15	2.10
1/2	.5	1	3.25	2.25
3/4	.5	1.5	3.35	2.40
1	.5	2	3.40	2.52
1 1/4	.5	2.5	3.50	2.66
1 1/2	.5	3	3.65	2.75
1 3/4	1	4	3.75	2.90
2	1	5	3.90	3.0
2 1/4	.5	5.5	4.00	3.10
2 1/2	1	6.5	4.10	3.25
3	2.5	9	4.30	3.40
3 1/2	2.5	11.5	4.40	3.60
4	2.5	14	4.55	3.75

^a ΔH_{cg} is the vertical deflection of the cg due to increased weight, accurate to $\pm 10\%$.

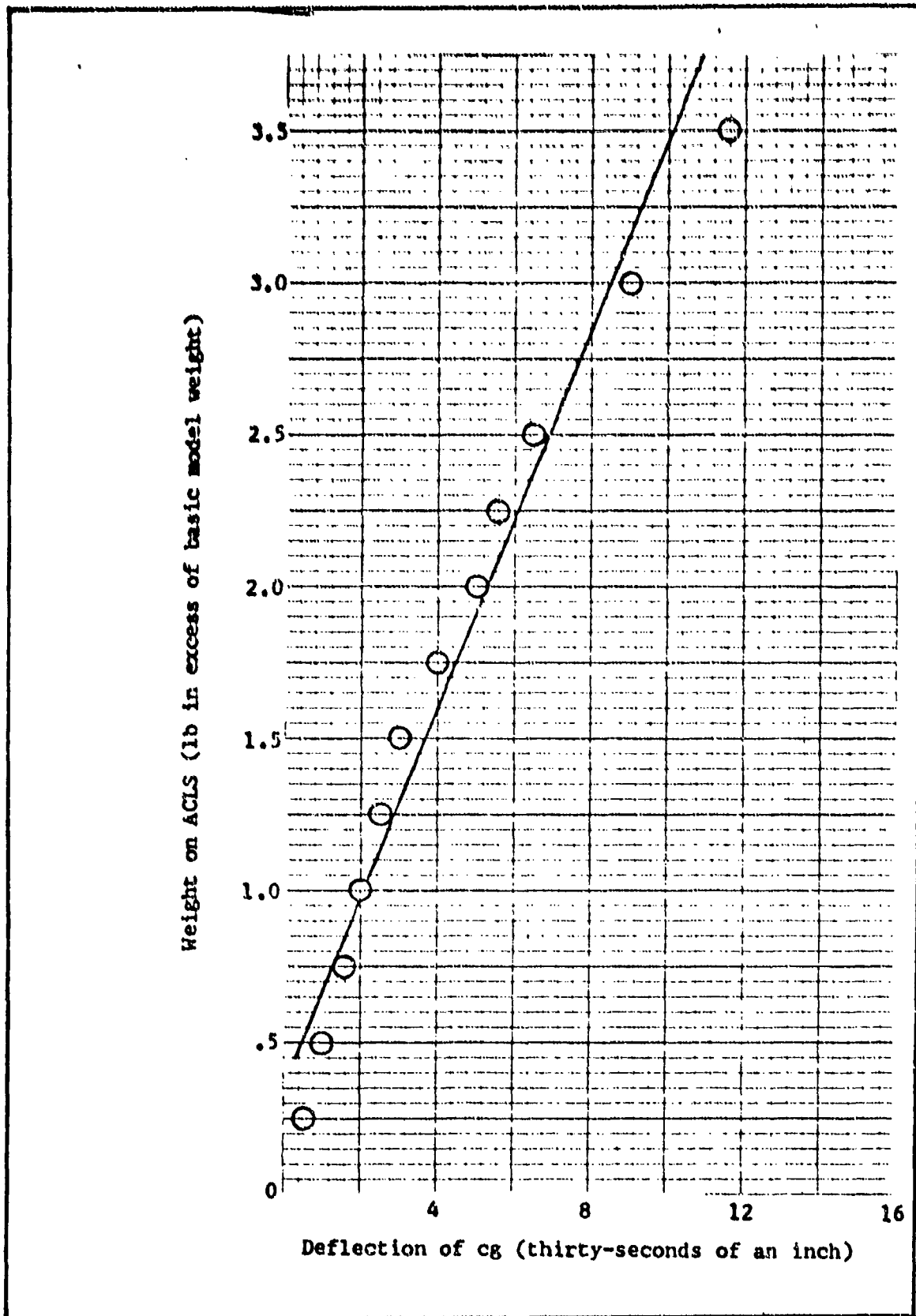


Fig. 14. Deflection of ACLS with Load for take off Configuration

Table VII

Deflection of cg with Increased Load for Take Off
Configuration, Air Cushion Vented

Weight (lb)	ΔH_{cg}^a (32nds in.)	Total ΔH_{cg} (32nds in.)	Trunk Pressure (in. H ₂ O)
0	0	0	4.30
1/2	1	1	5.15
1	1.5	2.5	5.30
1 1/2	1	3.5	5.40
2	2	5.5	5.45
2 1/2	2.5	8	5.45
3	2.5	10.5	5.45
3 1/2	2	12.5	5.45
4	3	15.5	5.45

^a ΔH_{cg} is the vertical deflection of the cg due to increased weight, accurate to $\pm 10\%$.

Table VIII

Results of Pull Tests

Configuration	P_t IGE (in. H ₂ O)	P_c IGE (in. H ₂ O)	Pull Force F_p (lb) ^a
Taxi/ Take Off (maximum air flow)	2.90	1.90	.02
Taxi/ Take Off brakes applied (air cushion vented)	4.75	.10	1.70-1.75
Normal Landing	4.75	1.80	.40-.45
Normal Landing brakes applied (air cushion vented)	5.0	.05	1.80-1.85

^aMeasurements accurate to $\pm .02$ lb for F_p less than 1 lb, accurate to $\pm .05$ lb for F_p greater than 1 lb.

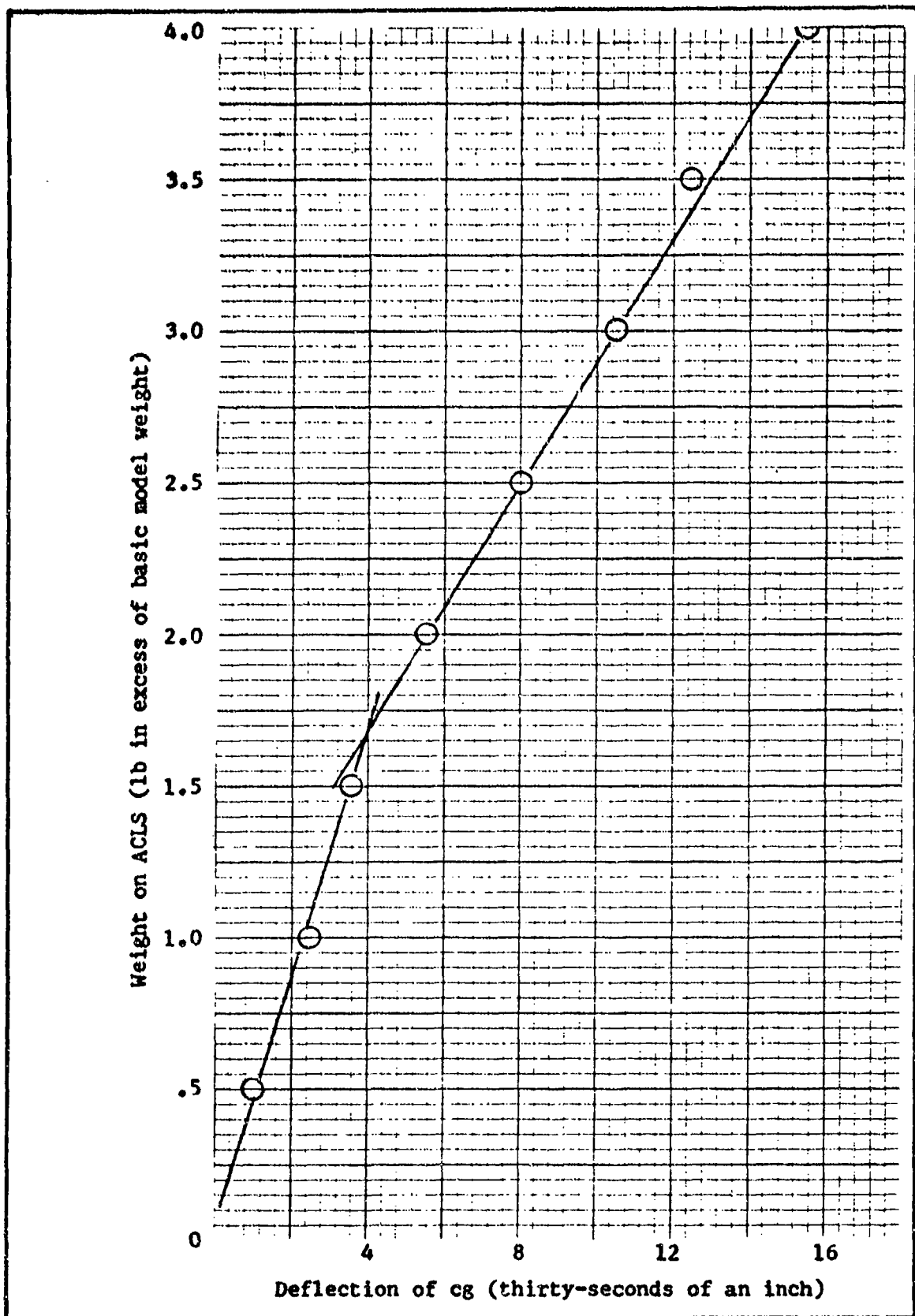


Fig. 15. Deflection of ACLS with Load for Cushion Vented Take off Config.

Table IXa

Roll Angle of ACLS for Positive Torque Applied
About the Longitudinal Axis

Note: Positive torque is that torque produced by weight on the right wing.

Number of Weights ^a	H _{WR} ^b (in.)	H _{WL} ^c (in.)	Roll Angle ϕ (deg)	Trunk Pressure (in. H ₂ O)	Cushion Pressure (in. H ₂ O)
0	3	3	0	4.75	1.75
1	2 23/32	3 9/32	1.47	4.75	1.85
2	2 15/32	3 17/32	2.77	4.75	1.80
3	2 6/32	3 26/32	4.4	4.75	1.70
4	1 29/32	4 1/32	5.55	4.75	1.60
5	1 19/32	4 10/32	7.1	4.75	1.40
6	1 8/32	4 19/32	8.75	4.75	1.30

^a Each weight weighed 8.4×10^{-3} lb \pm 3%.

^b Measured height of the right wingtip accurate to 1/32 in.

^c Measured height of the left wingtip accurate to 1/32 in.

Table IXb

Roll Angle of ACLS for Negative Torque Applied
About the Longitudinal Axis

Note: Negative torque is that torque produced by weight on the left wing.

Number of Weights ^a	H _{WR} ^b (in.)	H _{WL} ^c (in.)	Roll Angle ϕ (deg)	Trunk Pressure (in. H ₂ O)	Cushion Pressure (in. H ₂ O)
0	3	3	0	4.75	1.75
1	3 7/32	2 25/32	1.15	4.75	1.70
2	3 16/32	2 16/32	2.60	4.75	1.60
3	3 25/32	2 6/32	4.15	4.75	1.40
4	4 2/32	1 28/32	5.75	4.75	1.20
5	4 10/32	1 18/32	7.18	4.75	1.10
6	4 19/32	1 7/32	8.82	4.75	1.00

^a Each weight weighed 8.4×10^{-3} \pm 3%.

^b Measured height of the right wingtip accurate to 1/32 in.

^c Measured height of the left wingtip accurate to 1/32 in.

Table Xa

Pitch Angle of ACLS for Positive Torque Applied
About the Lateral Axis

Note: Positive torque is that torque produced by weight on the tail causing a nose high attitude

Number of Weights ^a	H _N ^b (in.)	H _T ^c (in.)	Pitch Angle Θ (deg)	Trunk Pressure (in. H ₂ O)	Cushion Pressure (in. H ₂ O)
0	3 21/32	2 20/32	2.27	4.75	1.80
1	3 23/32	2 16/32	2.68	4.75	1.80
2	3 26/32	2 12/32	3.15	4.75	1.60
3	3 28/32	2 8/32	3.57	4.75	1.45
4	3 30/32	2 4/32	3.98	4.75	1.25
5	4	2 2/32	4.26	4.75	1.10
6	4 2/32	1 29/32	4.74	4.75	.80
7	4 4/32	1 27/32	5.03	4.75	.65
8	4 6/32	1 24/32	5.37	4.75	.50

^aEach weight weighed 29 gm ± 3%

^bMeasured distance between tip of nose and surface accurate to 1/32 in.

^cMeasured distance between base of tail and surface accurate to 1/32 in.

Table Xb

Pitch Angle of ACLS for Negative Torque Applied
About the Lateral Axis

Note: Negative torque is that torque produced by weight on the nose causing a nose low attitude.

Number of Weights ^a	H _N ^b (in.)	H _T ^c (in.)	Pitch Angle Θ (deg)	Trunk Pressure (in. H ₂ O)	Cushion Pressure (in. H ₂ O)
0	3 20/32	2 22/32	2.07	4.75	1.80
1	3 18/32	2 24/32	1.78	4.75	1.80
2	3 16/32	2 26/32	1.52	4.75	1.75
3	3 13/32	2 28/32	1.17	4.75	1.60
4	3 10/32	2 30/32	.83	4.75	----
5	3 8/32	3	.55	4.75	1.35
6	3 6/32	3 2/32	.27	4.75	1.20
7	3 3/32	3 4/32	-.07	4.75	1.05
8	3	3 6/32	-.41	4.75	.80

Table XI
Results of Drop Tests Using Bell and Howell Accelerometer

Note: Full-scale vertical velocities simulated by drop heights are 7.5 fps, 11 fps and 14 fps.

Drop Height H _d (in.)	Peak Values			Time to Peak (ms)			Minimum Values		
	Trunk Pressure (in. H ₂ O)	Cushion Pressure (in. H ₂ O)	Load at cg (g)	P _t	P _c	a _{cg}	Trunk Pressure (in. H ₂ O)	Cushion Pressure (in. H ₂ O)	Load (g)
1.0 ^a	5.4	1.20	2.2	38	66	37	4.3	.60	.5
2.25	5.7	1.25	3.4	36	58	33	4.0	.40	.5
3.5	6.0	1.30	5.2	36	57	30	3.8	.25	.25

^aTests were conducted with ACLS in the normal landing configuration.

Table XII
Results of Drop Tests Using BBN-501 Accelerometer

Drop Height H _d (in.)	Peak Values		Load at cg (g)	Time to Peak (ms)			Minimum Values	
	Trunk Pressure (in. H ₂ O)	Cushion Pressure (in. H ₂ O)		P _t	P _c	a _{cg}	Trunk Pressure (in. H ₂ O)	Cushion Pressure (in. H ₂ O)
1.0 ^a	5.2	.80	2.3	42	75	30	4.1	.50
2.25	5.6	.90	3.2	42	71	30	3.8	.40
3.5	6.0	1.00	5	38	65	20	3.8	.30
1.0 ^b	5.4	.10	2.2	52	--	25	--	--
2.25	5.8	.20	2.3	48	--	25	--	--
1.0 ^c	1.4	.50	1.65	60	75	30	--	--
1.0 ^d	1.6	.10	2.0	60	--	30	--	--

^a ACLS in the normal landing configuration

^b ACLS in the landing configuration with air cushion vented

^c No air flow to the ACLS, air cushion vent closed

^d No air flow to the ACLS, air cushion vented

Table XIII

Braking Factor for Landings with Air Cushion Vented

Launch Velocity V_L (fps) $\pm 10\%$	Slide Out Distance (ft) $\pm 4\%$	Braking Factor ^a $\mu \pm 20\%$
11.4	6.7	.30
18.7	16.0	.34
26.4	35.2	.31
30.5	40.0	.36

^aAverage braking factor found to be .33. Error Analysis in Appendix F.

Table XIV

Theoretical Value of Air Cushion Area

Note: Braking factor was assumed to be the average μ computed for landings with the air cushion vented. P_c was assumed to be 1.0 in H_2O .

Launch Velocity (fps)	Slide Out Distance (ft)	Theoretical A_c (sq in)	Static ^a A_c (sq in)	Full Scale A_c (sq in $\times 10^{-2}$)
11.4	13.4	37.5	26	23.46
18.7	26.1	25.8	26	23.46
26.4	49.1	23	26	23.46

^aApproximate value of air cushion area computed for static operating conditions in the normal landing configuration.

Appendix F

Calculations and Error Analysis

Computation of Volumetric Flow Rate: The volumetric flow rate for the ACLS air supply system was computed from measurements of the trunk flow area and trunk pressure measured out of ground effect. It was assumed that the flow was steady, one dimensional, incompressible and obeyed the perfect gas law. The equations use the following symbols:

- \dot{m} is the mass flow rate.
- ρ_a is the density (assumed to be standard ambient density).
- u is the flow velocity from ports in the trunk.
- A_n is the actual trunk flow area.
- C_d is the discharge coefficient.
- Q is the volumetric flow rate.
- P_a is the ambient pressure.

$$\dot{m} = \rho_a A_n C_d u$$

It is assumed that the flow velocity in the trunk region is negligible. Solving Bernoulli's equation for u and using the fact that P_t (gage) equals P_t (absolute) minus P_a (absolute) gives the expression

$$\dot{m} = A_n C_d \sqrt{\frac{2P_t}{\rho_a}}$$

The volumetric flow rate is simply the mass flow rate divided by the density. After performing a dimensional analysis for the measured data and substituting the value of ρ_a , the expression used to calculate Q was

$$Q(\text{cfm}) = 272 C_d A_n (\text{in}^2) \sqrt{P_t (\text{in. H}_2\text{O})}$$

The errors in the value of Q come from errors in measuring the radii of the ports in the trunk and from errors in the measurement of trunk pressure. The average error in radius measurement was $\pm 5\%$. This made the average error in the area computation $\pm 10\%$. The error in P_c is small compared to the error in A_n , therefore the error in Q is taken to be the same as the error in the value of A_n .

Computation of Heave Stiffness Factor: The relation between the weight added to the model at the cg and the deflection of the cg was found to be nearly linear. The extended difference method was used to calculate the slope of the line. The value computed for the slope was then used as the heave stiffness factor K_h (lb per in.).

The errors in K_h come from errors in measuring the weight and the cg deflection ΔH_{cg} . The error in weight measurement is $\pm 1\%$. The error in measuring ΔH_{cg} was found to be 1.5%. The heave stiffness factor is equal to the unit weight divided by the deflection of the cg hence

$$\text{RMS error in } K_h = \sqrt{(\text{error in weight})^2 + (\text{error in } \Delta H_{cg})^2} = \pm 2\%$$

Computation of the Roll Stiffness Factor: The relation between the amount of weight applied to a wing and the resulting angular deflection was found to be linear. The slope was computed using the extended difference method. This value was multiplied by the moment arm (distance between the cg of the weights and the cg of the model) to find the roll stiffness factor K_θ .

$$K_\theta = \frac{\text{unit weight}}{\text{roll deflection}} \times \text{moment arm}$$

The error in the roll stiffness was made up of the errors in measuring the weights, the height of the wingtips and the moment arm. The weight measurement error K_w is $\pm 1\%$. The error in the measurement of the moment arm K_{ma} is $\pm 2.5\%$. The error in measuring the height of the wingtips is $\pm 1\%$. The angular deflection is computed from

$$\theta = \sin^{-1}\left(\frac{\Delta H_w}{b}\right) \pm \frac{\Delta H_w}{b}$$

where:

θ is the roll angle.

ΔH_w is the difference in the heights of the wingtips.

b is the span.

Since the error in the span measurement is less than the error in ΔH_w (.5% vs. 1.5%) the RMS error of θ is taken to be 1.5%. The value of the error in K_θ is computed from

$$\text{RMS Error in } K_\theta = \sqrt{(K_w)^2 + (K_\theta)^2 + (K_{ma})^2} = \pm 3\%$$

Computation of Pitch Stiffness Factor: The computation and error analysis of the pitch stiffness factor K_θ is exactly parallel to the computation and error analysis of the roll stiffness factor. The error in K_θ is found to be $\pm 3\%$.

Vertical Descent Rate: In computing the vertical descent rate V_v it was assumed that the model was in free fall from the release until the trunk contacted the surface. The computations employed the following relations:

$$H_d = \frac{at^2}{2}, \quad V_v = at$$

H_d is the drop height.

a is the acceleration of gravity.

t is the time from release until the trunk contacts the surface.

The errors involved come from the error in measuring H_d and the error from assuming a to be equal to 32.2 ft per sec². The RMS error in computing t is $\pm 1\%$. The RMS error that results for the estimate of V_v is less than $\pm 2\%$.

Computation for Launch Velocity: The full travel of the catapult carriage was timed 3 times and the average value was taken to be the time for full carriage travel. It was assumed that the acceleration of the carriage was constant and the same value for any carriage release point along the catapult rails. The acceleration of the carriage was computed from:

$$L_c = \frac{a_c t_c^2}{2} \quad \text{giving} \quad a_c = \frac{2L_c}{t_c^2}$$

where:

a_c is the acceleration of the carriage.

t_c is the time for full carriage travel.

L_c is the distance the carriage travels.

The launch velocity V_L was then computed using the relations:

$$t^2 = \frac{2L_c}{a_c} \quad , \quad V_L = a_c t = \sqrt{2a_c L_c}$$

where t as used above is the time required for the carriage to travel an arbitrary distance L_c .

The error in the launch velocity comes from the error in the computation of the acceleration and the error in measuring L_c .

The acceleration error comes primarily from the error in measuring t_0 which is nominally taken to be $\pm 10\%$ giving for the acceleration error:

$$\text{RMS acceleration error } K_a = \sqrt{(2 \times \text{error in } t_0)^2} = \pm 20\%$$

The error in V_L is due primarily to K_a so that:

$$\text{RMS error in } V_L = \sqrt{\left(\frac{K_a}{2}\right)^2} = \pm 10\%$$

Computation of Brake Factor: The drag force on the model during slide out equals the mass of the model times the deceleration of the model. The drag also equals the braking coefficient or braking factor μ times the weight on the braking surface. It was assumed that the deceleration of the model was constant. The deceleration a_d was computed in the following manner:

$$\text{final velocity} = 0 = a_d t + V_L$$

$$t = \left| \frac{V_L}{a_d} \right| \quad \text{where } t \text{ is time from touchdown until stop}$$

$$\text{landing distance } d_s = V_L t = \frac{a_d t^2}{2}$$

$$\text{solving for } a_d, \quad a_d = \frac{-V_L^2}{2d_s}$$

The weight on the braking surface is the weight of the model, minus the upward force of the air cushion ($P_{C A_C}$) minus the aerodynamic lift. For the air cushion vented configuration, the last two values were assumed to be negligible giving the model weight W_m to be the weight on the braking surface. The braking factor μ was then computed using:

$$\text{Drag} = \left(\frac{W_m}{R_c} \right) a_d = \mu W_m$$

$$\text{substituting for } a_d, \mu = \frac{V_L^2}{2d_s R_c}$$

The RMS error in μ comes primarily from the error in V_L of $\pm 10\%$.

$$\text{RMS error in } \mu = \sqrt{(2 \times \text{error in } V_L)^2} = \pm 20\%$$

Check of the Braking Factor Computations by Computing a Theoretical Value of Λ_c : The average value of μ was used to compute the air cushion area Λ_c . The weight on the braking surface was assumed to be the weight of the model minus the upward force from the air cushion $P_c \Lambda_c$. This was used in the relation for the drag.

$$\text{Drag} = \left(\frac{W_m}{R_c} \right) a_d = \mu (W_m - P_c \Lambda_c)$$

$$\text{substituting for } a_d \text{ gives } P_c \Lambda_c = W_m - \left(\frac{W_m V_L^2}{2\mu R_c d_s} \right)$$

P_c was nominally chosen to be 1.0 in. H_2O and the theoretical value of Λ_c was computed using the relation above.

VITA

Philip M. Parker, Jr. was born on August 18, 1943 in Buffalo, New York, the son of Philip M. and Laura L. Parker. He received a Congressional appointment to the United States Air Force Academy and graduated in 1965 with a B.S. in Engineering Science and a commission as a 2nd Lt in the U. S. Air Force. He attended pilot training at Laredo AFB Texas and received his wings in September 1966. He served in tactical fighters in the 33rd Tactical Fighter Wing at Eglin AFB, Florida and the 13th Tactical Fighter Squadron at Udorn RTAFB, Thailand. He returned to Laredo AFB in August 1968 and served there as an instructor pilot until his assignment to AFIT in June 1972. Capt Parker is married to the former Lou Cinda Marie Stevenson and has a daughter, Kimberly Anne age 4 and a son Brian Scott age 3.